ARTICLE

DCIR and its ligand asialo-biantennary N-glycan regulate DC function and osteoclastogenesis

Tomonori Kaifu[1,2]* , Rikio Yabe[1]* , Takumi Maruhashi[1,3]* , Soo-Hyun Chung[1,2]* , Hiroaki Tateno[4] , Noriyuki Fujikado[1,2] , Jun Hirabayashi[4] , and Yoichiro Iwakura[1,2]

Dendritic cell immunoreceptor (DCIR) is a C-type lectin receptor with a carbohydrate recognition domain and an immunoreceptor tyrosine-based inhibitory motif. Previously, we showed that *Dcir*^{−/−} mice spontaneously develop autoimmune enthesitis and sialadenitis, and also develop metabolic bone abnormalities. However, the ligands for DCIR functionality remain to be elucidated. Here we showed that DCIR is expressed on osteoclasts and DCs and binds to an asialo-biantennary N-glycan(s) (NA2) on bone cells and myeloid cells. Osteoclastogenesis was enhanced in *Dcir*^{−/−} cells, and NA2 inhibited osteoclastogenesis. Neuraminidase treatment, which exposes excess NA2 by removing the terminal sialic acid of N-glycans, suppressed osteoclastogenesis and DC function. Neuraminidase treatment of mice ameliorated collagen-induced arthritis and experimental autoimmune encephalomyelitis in a DCIR-dependent manner, due to suppression of antigen presentation by DCs. These results suggest that DCIR activity is regulated by the modification of the terminal sialylation of biantennary N-glycans, and this interaction is important for the control of both autoimmune and bone metabolic diseases.

Introduction

Dendritic cell (DC) immunoreceptor (DCIR, or DCIR1; gene symbol, *Clec4a2*) is a member of the C-type lectin receptors. DCIR contains a carbohydrate recognition domain (CRD) in the extracellular part, which can recognize mono- and oligosaccharide structures in a Ca²⁺-dependent manner. The DCIR CRD has an EPS (glutamic acid–proline–serine) motif similar to the authentic carbohydrate recognition EPN (glutamic acid–proline–asparagine) motif that binds mannose, glucose, GlcNAc, and fucose. Several molecules, including asialo-N-glycans, were reported to bind DCIR (Bloem et al., 2014; Bloem et al., 2013; Hsu et al., 2009; Lee et al., 2011; Massoud et al., 2014; Nasu et al., 2020). However, the effects of these glycans on DCIR functions have yet to be examined.

DCIR has a canonical immunoreceptor tyrosine-based inhibitory motif (ITIM) in the cytoplasmic portion (Graham and Brown, 2009), which transduces inhibitory signals by activating phosphatases SHP-1 and SHP-2 upon stimulation (Richard et al., 2006). Previously, we showed that aged *Dcir*^{−/−} mice spontaneously

develop autoimmune enthesitis and sialadenitis, because antigen presentation ability of the immune system is enhanced due to excess differentiation and proliferation of DCs in *Dcir*^{−/−} mice (Fujikado et al., 2008). Furthermore, *Dcir*^{−/−} mice are highly susceptible to collagen-induced arthritis (CIA; Fujikado et al., 2008), a model for rheumatoid arthritis (Brand et al., 2007), and experimental autoimmune encephalomyelitis (EAE; Seno et al., 2015), a model for multiple sclerosis (Stromnes and Goverman, 2006), respectively, indicating an important regulatory role of DCIR in the immune system.

We also found that ankylotic changes of the ankle joints develop in *Dcir*^{−/−} mice with age due to fibrocartilage proliferation and heterotopic ossification in joints, associated with an increase in the femoral bone mass (Fujikado et al., 2008; Maruhashi et al., 2015). This is because T helper type 1 cell differentiation is enhanced in *Dcir*^{−/−} mice, and overproduced IFN-γ from T helper type 1 cells promotes chondrogenesis and bone formation (Maruhashi et al., 2015). Thus, DCIR plays important regulatory

roles in both the immune system and the bone metabolic system. However, the regulatory mechanisms of DCIR activity remain obscure.

In this study, we showed that an endogenous asialo-biantennary N-glycan (NA2) can bind DCIR. By analyzing the effects of NA2 on osteoclastogenesis, we identified NA2 as a functional ligand for mouse and human DCIR. Furthermore, we showed that exposure of NA2 on the cell surface by removing the terminal sialic acid of N-glycans with sialidases suppresses osteoclastogenesis and DC maturation by acting on DCIR on the cell surface. Sialidase treatment also suppressed the development of CIA and EAE. These findings suggest that the NA2-DCIR axis is critically important for the homeostasis of the immune and bone system.

Results

DCIR ligands are expressed on macrophages, osteoclasts and osteoblasts

To identify the functional ligands of DCIR, we generated DCIR-Fc, in which the extracellular domain (EC) of DCIR was fused with the Fc region of human IgG2, and examined the binding of DCIR-Fc to different types of cells. Although T and B lymphocytes did not bind to DCIR-Fc (data not shown), a portion of macrophages was positive for DCIR-Fc staining (Fig. S1, a and b). Osteoclasts, which are differentiated from the cells in the monocyte-macrophage lineage, were also partially positive for DCIR-Fc staining (Fig. S1, c and d). The binding was reduced with DCIRE197A/S199A-Fc, a mutant DCIR-Fc with two point mutations in EPS (Zelensky and Gready, 2005; Fig. S1, a and b). Moreover, since less binding was observed after treatment of macrophages with EDTA or trypsin, it was determined that DCIR interacts with glycoproteins on macrophages and osteoclasts in a CRD- and Ca²⁺-dependent manner (Fig. S1, a and b). Since osteoclast differentiation is tightly regulated by osteoblasts (Lee et al., 2010), we investigated whether DCIR ligands were presented on osteoblasts. Osteoblasts were positive for DCIR-Fc staining, and a reduction in binding occurred in the presence of EDTA (Fig. S1 e). As is the case with macrophages and osteoclasts, the binding of DCIR-Fc to osteoblasts was dependent on the EPS motif (Fig. S1 f). To further characterize the DCIR ligands, osteoblasts were treated before DCIR-Fc staining with tunicamycin, which blocks N-linked glycosylation, and benzyl-α-GalNAc, which inhibits O-linked glycosylation. The binding of DCIR-Fc was abolished after treatment with tunicamycin, but not benzyl-α-GalNAc (Fig. S1 g), indicating that DCIR ligands are likely to be N-linked glycans on glycoproteins.

NA2 specifically binds DCIR

Since N-linked glycans were considered to be a potential ligand for DCIR, a glycan microarray with the evanescent-field fluorescence-assisted detection system (Tateno et al., 2008) was used to screen the saccharide ligands using the DCIR-Fc protein as the probe. By exploiting this system, it was possible to detect weak interactions with high sensitivity. The glycan microarray revealed that DCIR-Fc bound to asialo-transferrin and heparin in a Ca²⁺-dependent manner, but not to glycoproteins

expressing high mannose-type glycans, highly branched complex-type N-linked glycans, fucosylated glycoconjugates, or O-linked glycans that were spotted on the array (Fig. S2). DCIR-Fc bound to asialo-transferrin and heparin in a dose-dependent manner, and EDTA completely blocked the binding (Fig. 1 a). No binding of mutant DCIR-Fc (E197A-Fc, S199A-Fc, and E197A/S199A-Fc) to asialo-transferrin was observed, whereas the mutant DCIR-Fcs remained to bind heparin (Fig. 1 b). Because the binding of DCIR-Fc depended on CRD, and it was considered likely that N-linked glycans were the ligands for DCIR (Fig. S1), we focused on identifying the DCIR ligand on asialo-transferrin. Since the biantennary structure of N-glycans including NA2 is predominant on transferrin (Regoeczi et al., 1979), we tested the binding of DCIR-Fc to NA2. As shown in Fig. 1, c and d, DCIR-Fc bound strongly to NA2 in a Ca²⁺- and CRD-dependent manner. As human and mouse DCIR have 65% homology of the amino acid sequences over the whole sequence with the EPS motif in the EC, we examined the binding of human DCIR to NA2. As shown in Fig. 1 e, human DCIR-Fc also bound to NA2 in a Ca²⁺-dependent manner.

It has been shown that DCIR can bind to the glycans expressed by Chinese hamster ovary (CHO) cells (Bloem et al., 2013). Therefore, we examined DCIR-Fc binding to glycan transporter–deficient CHO cells. The binding of DCIR-Fc was strongly enhanced in Lec2 cells that expressed sialic acid–deficient complex N-glycans due to the lack of cytidine 5′-monophosphate–sialic acid transporters compared with the parental CHO cells (Fig. 1 f). However, no binding was detected on Lec8 cells, which expressed sialic acid/galactose–deficient complex N-glycans due to the lack of uridine 5′-diphophate–galactose transporters, or on the Lec1 cells, which lack complex and hybrid-type N-glycans due to defective N-acetylglucosaminyltransferase I.

To obtain further structural insight into the importance of the biantennary structure and desialylated forms, we transfected 293T cells, which expressed a low level of the DCIR ligand, with Mgat2 (β-1, 2-N-acetylglucosaminyltransferase II) to transfer GlcNAc to the β1-2 of Manα1-6 (GlcNAcβ1-2Manα1-3) Manβ1-4GlcNAcβ1-4GlcNAcβ1-Asn in order to achieve an overexpression of NA2. Although nontransfected 293T cells were not bound to DCIR-Fc, Mgat2-293T cells were clearly positive for DCIR-Fc (Fig. 1 g). These results confirm that mouse and human DCIR interact with the desialylated biantennary structures of N-glycans.

DCIR negatively regulates osteoclastogenesis

Because DCIR is highly expressed in myeloid-lineage cells, such as DCs and macrophages, and Dcir⁻/⁻ mice develop bone abnormalities, we next examined the expression of DCIR in osteoclasts, one of the myeloid lineage cells. Osteoclasts originate from hematopoietic stem cells in bone marrow (BM), and both the macrophage CSF (M-CSF) and receptor activator of NF-κB ligand (RANKL) are critically important for the differentiation of osteoclasts (Negishi-Koga et al., 2011; Okamoto and Takayanagi, 2019; Pederson et al., 2008). In addition, an immunoreceptor tyrosine-based activation motif–mediated signal is a requirement for terminal osteoclast formation, and is counterbalanced by phosphatases (Kaifu et al., 2003; Koga et al., 2004; Takeshita
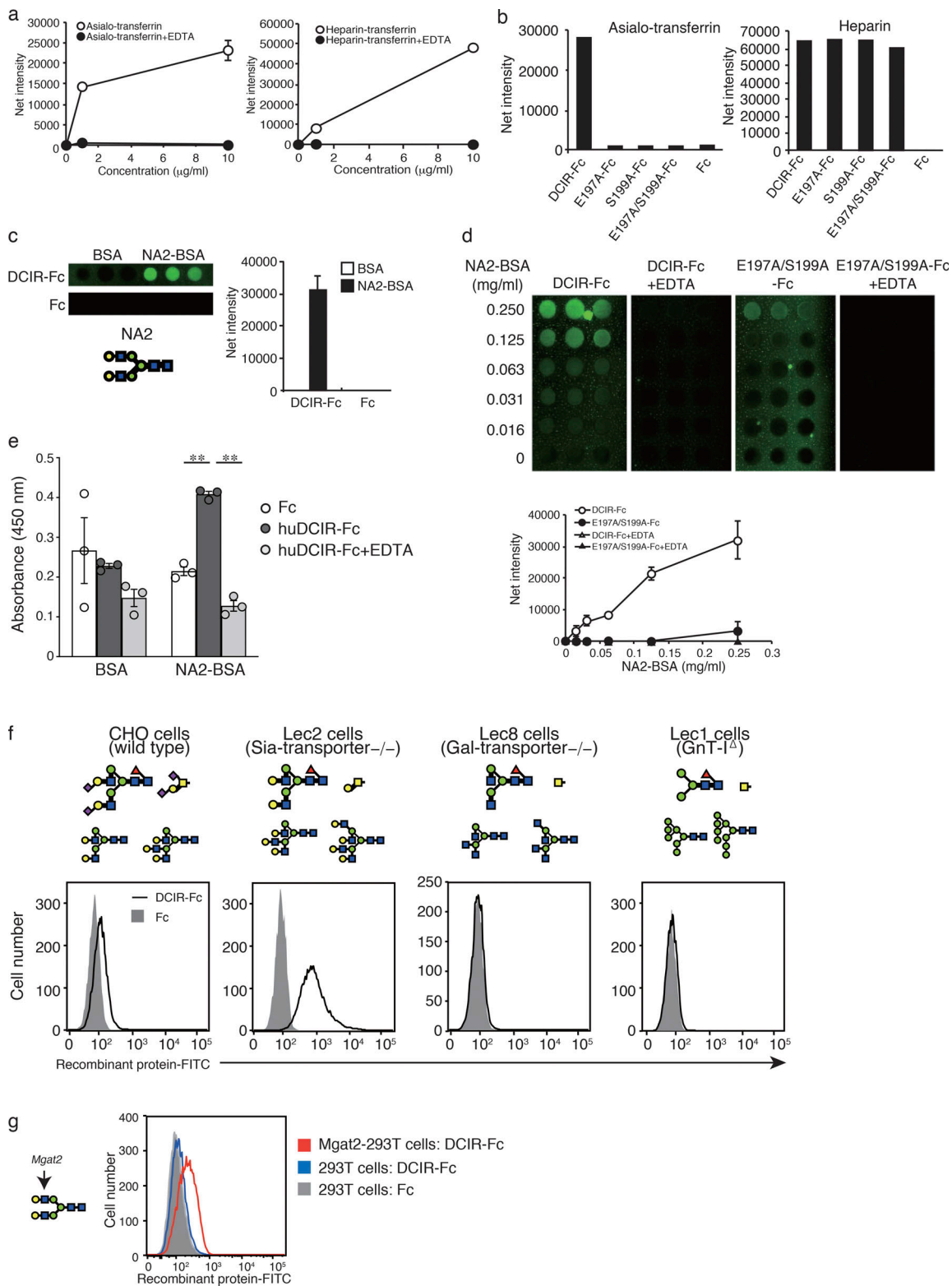
Kaifu et al.
The DCIR-NA2 in the immune and bone system

Journal of Experimental Medicine   2 of 20
https://doi.org/10.1084/jem.20210435

Figure 1. **NA2 can bind DCIR.** **(a)** Ca^{2+}- and dose-dependency of DCIR-Fc binding to plate-coated asialo-transferrin and heparin. Bound DCIR-Fc was detected by FITC-conjugated anti-human IgG. **(b)** CRD dependency of DCIR-Fc binding to asialo-transferrin and heparin was assessed using DCIR-Fc, single mutant DCIR-Fc (E197A-Fc), and double mutant DCIR-Fc (E197A/S199A-Fc). **(c)** Binding of DCIR-Fc to NA2-BSA in a glycan microarray assay. **(d)** Ca^{2+}- and CRD-dependency of DCIR-Fc binding to NA2-BSA. **(e)** Binding of human DCIR-Fc to NA2-BSA in a solid phase binding assay. The bar represents the mean ± SEM. **, P < 0.01 (one-way ANOVA with Dunnett's post hoc test). **(f)** The structure of N-linked glycans that are expressed in CHO cells and their derivatives (top), and DCIR-Fc binding to these cells (bottom). Desialylated bi-antennary structure is required for DCIR-Fc binding. Data are the mean ± SD of triplicate spots (a–d). **(g)** Binding of DCIR-Fc to Mgat2-transfected 293T cells and 293T cells. The quantification of net intensity was determined by the signal intensity minus background intensity (a–d). The data are representative of at least two independent experiments (a–g).

et al., 2002; Umeda et al., 1999). We found that DCIR was expressed in M-CSF– and RANKL-induced osteoclasts (Fig. 2 a) and M-CSF–induced BM macrophages (BMMs; Fig. S2, b and c). Its expression progressively increased during osteoclast maturation. DCIR was also detected in CD11b-positive OsteoMacs (Chang et al., 2008), but not in osteoblasts (Fig. S2 d).

We examined the role of DCIR in osteoclastogenesis in an in vitro culture system. When osteoclasts were induced to differentiate from BMMs with M-CSF and RANKL, $Dcir^{-/-}$ BMMs formed tartrate-resistant acid phosphatase (TRAP)–positive osteoclasts with >10 nuclei, making them more efficient than WT BMMs (Fig. 2 b). The expression of osteoclastic genes, such as $Nfatc1$ (a master regulator of osteoclast formation), $Acp5$ (an enzymatic marker of osteoclasts), Src (a tyrosine kinase essential for bone resorption), $Calcr$ (a receptor for calcitonin), and $Ctsk$ (a protease responsible for degrading type I collagen), was significantly increased in $Dcir^{-/-}$ osteoclasts (Fig. 2 c). Osteoclast differentiation was significantly suppressed by the retroviral expression of DCIR, but not by an ITIM mutant (DCIRY7F) that lacked the ability to deliver inhibitory signaling, indicating that ITIM-mediated signaling is required for the DCIR-induced suppression of osteoclastogenesis (Fig. 2 d). Furthermore, multinucleated osteoclast formation was also enhanced when nonadherent $Dcir^{-/-}$ BM cells (BMCs) were cocultured with WT osteoblasts, but not vice versa, indicating that DCIR is a unique inhibitory receptor that down-regulates osteoclastogenesis (Fig. 2 e).

NA2 is a functional DCIR ligand that negatively regulates osteoclastogenesis

We investigated the effect of NA2, putative DCIR ligands, on osteoclastogenesis. When WT BMMs were induced to differentiate with M-CSF and RANKL in the presence of DCIR-Fc, which blocks the interaction between DCIR and its ligand, a significant increase in the number of TRAP+ multinucleated cells was observed (Fig. 3 a). However, a mutant form of DCIR-Fc, DCIRE197A/S199A-Fc, had no effect at all, indicating that the effect of DCIR-Fc on osteoclastogenesis depends on the CRD. DCIR-Fc had no effect on osteoclast formation from $Dcir^{-/-}$ BMMs (Fig. 3 a). Consistent with this observation, multinucleated TRAP+ osteoclast formation was strongly inhibited by treatment with NA2 in the WT BMM culture, but not in the $Dcir^{-/-}$ BMM culture (Fig. 3 b). In addition, we examined the effect of NA2 on the osteoclastogenesis of human cells. Osteoclast formation was significantly suppressed by the treatment with NA2 of human CD14+ cells from peripheral blood (Fig. 3 c), indicating that NA2 is also the functional ligand for human DCIR to regulate osteoclastogenesis.

Because the binding of DCIR-Fc was increased in Lec2 cells, which lack terminal sialic acid in complex N-glycans (Fig. 1 e), we next examined the effect of neuraminidase treatment, which results in more desialylated glycans on the cell surface, on the binding of DCIR-Fc. Interestingly, neuraminidase treatment of BMMs enhanced the binding of DCIR-Fc, but not DCIRE197A/S199A-Fc (Fig. 3, d and e). Furthermore, RANKL-induced osteoclast formation was drastically inhibited by the treatment with neuraminidase in WT BMMs, but no such effect was noted in

$Dcir^{-/-}$ BMMs (Fig. 3 f). Neuraminidase treatment also suppressed multinucleated osteoclast formation in WT cells, but not in $Dcir^{-/-}$ cells in a nonadherent BMC and osteoblast co-culture system (Fig. 3 g). β-Galactosidase treatment did not affect osteoclast formation in WT cells and $Dcir^{-/-}$ cells, indicating that the terminal galactose in complex N-glycans is involved in the recognition by DCIR.

We examined the effect of neuraminidase treatment on modifying bone metabolism in vivo. First, we evaluated DCIR-Fc binding to BMCs after in vivo treatment with neuraminidase. 1 d after neuraminidase administration, DCIR-Fc–positive cells in BMCs were higher than those injected with PBS (Fig. S3, a and b), showing that the neuraminidase treatment enhanced exposure of NA2 on the cell surface by removing the terminal sialic acids of N-glycans.

To examine the osteoclast activity after the intravenous injection of neuraminidase, we measured the calcium ion concentration and TRAP activity in sera. While the concentration of calcium ions and the phosphatase activity were significantly reduced in WT, this was not observed in $Dcir^{-/-}$ mice after neuraminidase treatment (Fig. 3, h and i). These observations are consistent with the notion that excess NA2 exposure suppressed osteoclast activity in a DCIR-dependent manner. Thus, we conclude that NA2 is a functional and specific DCIR ligand that negatively regulates osteoclastogenesis.

Intravenous administration of neuraminidase suppresses the development of CIA

Since DCIR negatively regulates the development of CIA (Fujikado et al., 2008), we analyzed the effect of administering neuraminidase on the development of this disease. We used DBA/1J mice, because these mice are more susceptible to CIA than C57BL/6J mice. When CIA was induced after treatment with neuraminidase, the arthritic score was significantly lower than that of PBS-treated mice (Fig. 4 a). The cumulative arthritic score and mean maximal score were also suppressed, while the incidence, mean maximal score, and disease onset time were not significantly affected in neuraminidase-injected mice (Fig. 4 b). We also assessed the histological parameters. The reduction in the inflammatory score, pannus formation, cartilage erosion, and bone destruction was much more pronounced in neuraminidase-treated mice than in PBS-treated mice (Fig. 4, c and d). A significant decrease in the serum concentration of IFN-γ and IL-17A, but not of IL-6, was noted at the end of clinical monitoring in neuraminidase-treated mice (Fig. 4 e). To examine the effect of neuraminidase on bone resorption during CIA, we measured the serum concentration of type I collagen C-terminal telopeptide (CTX-I), which is produced by cathepsin K from type I collagen. The concentration of CTX-I in the serum of neuraminidase-treated DBA/1J mice was significantly lower than in PBS-treated mice (Fig. 4 f). Because osteoclasts mediate bone destruction in CIA, TRAP+ cells were quantified in joint sections. Neuraminidase treatment significantly decreased osteoclast numbers in joints (Fig. 4, g and h).

We next analyzed the effects of neuraminidase treatment on $Dcir^{-/-}$ mice to examine dependency on DCIR. When neuraminidase was injected intravenously into C57BL/6J mice, the
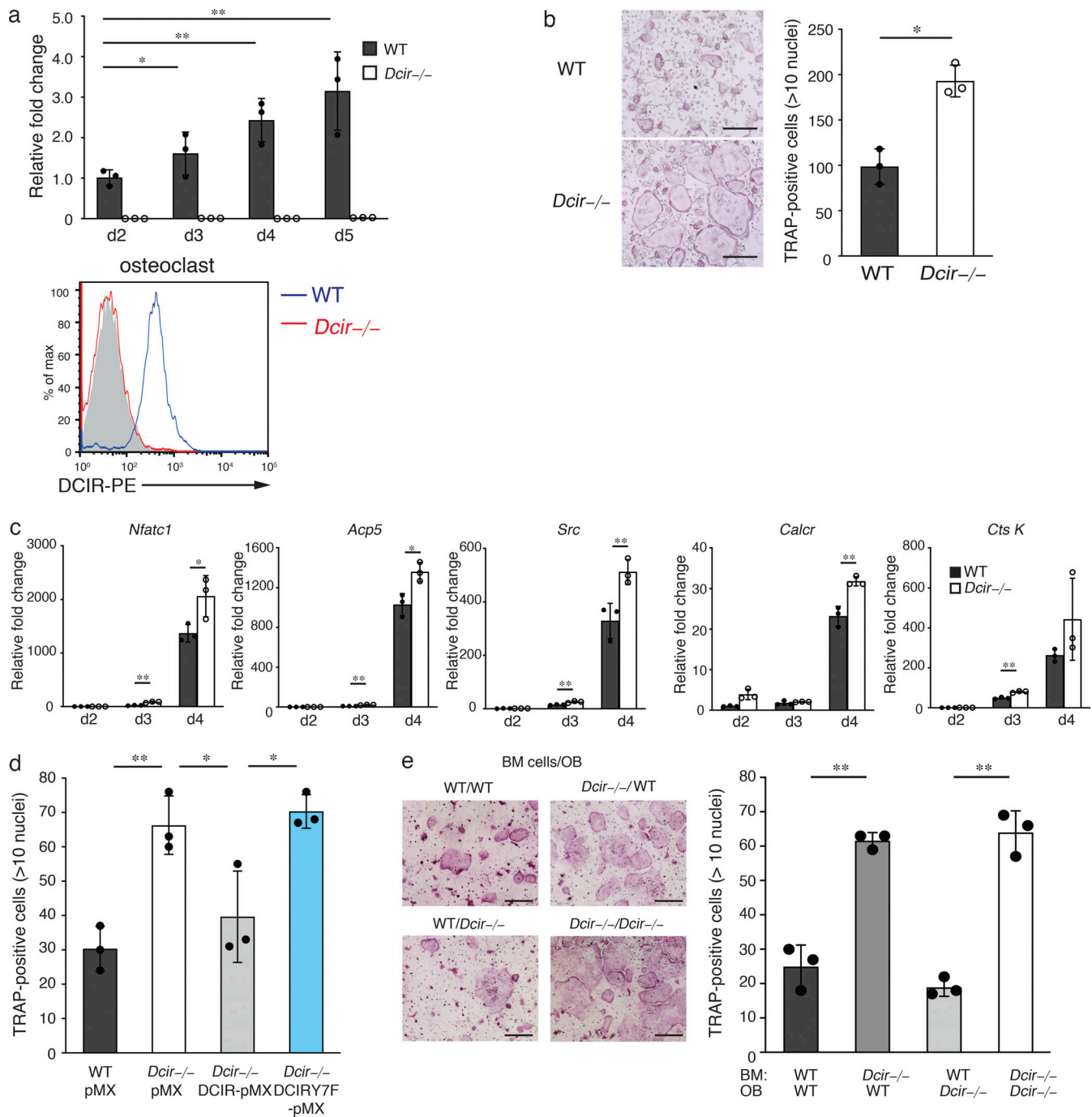
Figure 2. **DCIR deficiency enhances in vitro osteoclastogenesis. (a)** After osteoclastogenesis was induced in WT and $Dcir^{-/-}$ BMMs with M-CSF (20 ng/ml) and RANKL (100 ng/ml), DCIR mRNA expression was measured by quantitative PCR periodically (top). DCIR expression on osteoclasts was also examined by FACS using an anti-Clec4a antibody 4 d after M-CSF + RANKL activation (bottom). **(b)** The number of TRAP⁺ multinucleated (>10) osteoclasts was counted in WT and $Dcir^{-/-}$ BMMs culture 3 d after M-CSF + RANKL activation. Scale bar, 300 μm. **(c)** Expression of osteoclastogenic genes was analyzed by quantitative PCR on the indicated days after osteoclastogenesis induction. Relative values to WT mRNA expression at day 2 are shown. **(d)** WT or $Dcir^{-/-}$ BMs were infected with retroviruses carrying either none (pMX vector), or WT DCIR-pMX-, or ITIM-deficient DCIRY7F-pMX, and TRAP⁺ cells were examined after 5 d. **(e)** Non-adherent BMCs (BM) and osteoblasts (OB) were cocultured, and the effect of $Dcir$ deficiency on osteoclast formation was examined after 7 d. Scale bar, 300 μm. The data are representative of two (d) or three independent experiments (a–c and e). The error bars show the mean ± SD of triplicate cultures. The Fc portion of human IgG2 was used as a negative control for Fc-DCIR. Statistical significances (*, $P < 0.05$; **, $P < 0.01$) are evaluated by the two-tailed unpaired Student's t test (b, c, and e) and one-way ANOVA with Dunnett's post hoc test (a and d).
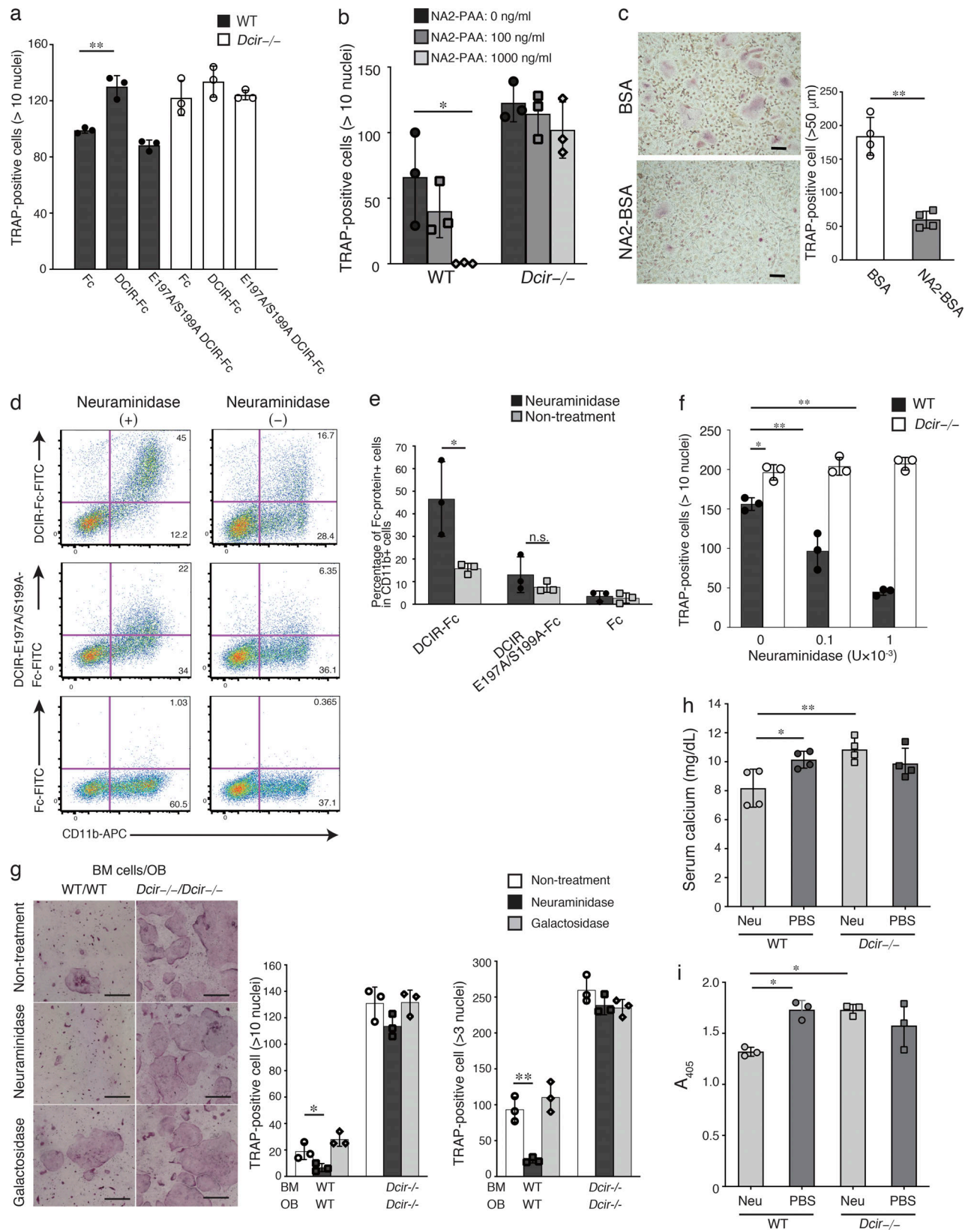
Figure 3. **NA2 is a functional DCIR ligand capable of activating DCIR. (a)** Osteoclastogenesis was induced in WT and *Dcir*^{−/−} BMMs with M-CSF (20 ng/ml) and RANKL (100 ng/ml) in the presence or absence of Fc, DCIR-Fc, or mutant DCIR-Fc, and osteoclast differentiation was examined after 5 d. Data are representative of two independent experiments. Data denote the mean ± SD of triplicate cultures. **(b)** Osteoclast differentiation was induced in BMMs from WT or *Dcir*^{−/−} BMCs by culturing with M-CSF and RANKL in the presence of indicated concentrations of NA2-PAA, and osteoclast differentiation was examined after 5 d. **(c)** Osteoclast differentiation from human peripheral blood CD14^{+} cells in the presence of NA2-BSA. Osteoclast differentiation was examined after

8 d. **(d and e)** BMMs were induced to differentiate in the presence or absence of neuraminidase (0.1 U/ml; Roche), and DCIR-Fc binding was examined after 6 d by FACS. Representative flow cytometry plots of BMMs. Data denote the mean ± SEM of three independent experiments. **(f)** Osteoclastogenesis was induced in WT and $Dcir^{-/-}$ BMMs with M-CSF and RANKL in the presence or absence of indicated concentrations of neuraminidase, and TRAP+ osteoclasts were counted after 5 d. **(g)** Osteoclastogenesis was induced in WT and $Dcir^{-/-}$ BMMs in BMC (BM) and osteoblast (OB) co-culture in the presence or absence of neuraminidase (0.1 U/ml) or galactosidase (20 mU/ml), which catalyzes the removal of a β-galactose residue from polysaccharides, and TRAP+ osteoclasts were counted after 7 d. Data are the mean ± SD of triplicate cultures. Scale bar, 300 μm. The data are representative of at least three independent experiments (f and g). **(h)** Serum calcium ion concentration was determined 10 d after the intravenous injection of neuraminidase (0.1 U/mouse) in WT and $Dcir^{-/-}$ male mice ($n = 4$). **(i)** Serum TRAP activity was measured 10 d after the intravenous injection of neuraminidase (0.1 U/mouse) in WT and $Dcir^{-/-}$ male mice ($n = 5$). Data are representative of two independent experiments (h and i). The bars present the mean ± SEM. Statistical significances (*, $P < 0.05$; **, $P < 0.01$) are evaluated by the two-tailed unpaired Student's t test (c and e) and one-way ANOVA with Dunnett's post hoc test (a, b, and f–i).

arthritic scores, but not the incidence of arthritis, of neuraminidase-treated WT mice were significantly lower than those of PBS-treated WT mice, whereas the injection had no effect on the arthritic scores of $Dcir^{-/-}$ mice (Fig. 5 a). The cumulative arthritic score and mean maximal score, but not the disease onset time, were also significantly suppressed, compared with those of PBS-treated mice (Fig. 5 b). Histological assessments showed that both leukocyte infiltration and pannus formation were ameliorated in neuraminidase-treated WT mice compared with PBS-treated WT mice, whereas both parameters were high in $Dcir^{-/-}$ mice irrespective of neuraminidase treatment (Fig. 5, c and d). The scores for cartilage and bone damage in neuraminidase-treated WT, but not $Dcir^{-/-}$, mice showed a similar tendency, although the differences were not statistically significant (cartilage damage, $P = 0.86$; bone damage, $P = 0.45$; Fig. 5, c and d). Also, no significant change was observed in the anti-collagen antibody titers in these mice (Fig. S3 c). Furthermore, serum concentration of CTX-I in neuraminidase-treated WT mice was lower than in PBS-treated WT mice, but the injection had no effects on the CTX-I concentration of $Dcir^{-/-}$ mice (Fig. 5 e). Consistent with this, TRAP+ cells were more significantly decreased in neuraminidase-treated WT mice than those of PBS-treated WT mice (Fig. 5, f and g). These results suggest that neuraminidase treatment causes excess exposure of NA2 and attenuates the development of CIA through the activation of DCIR.

Neuraminidase treatment of mice suppresses the development of EAE

In an earlier study by our group, we reported that the deficiency of DCIR exacerbates the development of EAE, indicating that DCIR is involved in the suppression of autoimmunity (Seno et al., 2015). Then, we examined the effects of neuraminidase treatment during the development of EAE. Neuraminidase injection in C57BL/6J mice significantly ameliorated the development of EAE compared with PBS-treated WT mice, and this treatment had no effect on $Dcir^{-/-}$ mice (Fig. 6 a). Cumulative clinical score and maximum score were significantly reduced in neuraminidase-treated WT mice, but disease onset time was comparable between neuraminidase- and PBS-treated mice (Fig. 6 b). Histological analysis also showed that leukocyte infiltration was reduced in neuraminidase-treated WT mice, while leukocyte infiltration in $Dcir^{-/-}$ mice was comparable in both neuraminidase- and PBS-treated mice (Fig. 6 c). Histological score in neuraminidase-treated WT mice was lower than in PBS-treated WT mice (Fig. 6 d). Moreover, Kluver–Barrera (KB)

staining showed that the state of demyelination, which is weaker pale blue area containing blue violet dots in the white matter, was significantly ameliorated in neuraminidase-treated WT mice (Fig. 6, e and f). However, neuraminidase treatment didn't mitigate demyelination in $Dcir^{-/-}$ mice, indicating that interaction of DCIR with NA2 alleviates immune responses to self-antigens.

The antigen-presenting ability of DCs is impaired by the treatment with neuraminidase

Since immune responses were suppressed by excess DCIR signaling with neuraminidase treatment, we next examined the effect of neuraminidase treatment on DC-mediated T cell response. To determine whether DCs possess DCIR ligands, we differentiated DCs from BMCs with GM-CSF (GM-DCs) and evaluated the DCIR-Fc binding to GM-DCs, which were treated by neuraminidase before the biding assay. DCIR-Fc binding to GM-DCs was significantly increased after neuraminidase treatment, indicating that neuraminidase treatment enhanced ligand exposure on GM-DCs (Fig. 7 a). However, GM-DC cell number did not change between neuraminidase-treated and nontreated DCs during differentiation, suggesting that neuraminidase treatment did not affect GM-DC growth or survival (Fig. 7 b).

We analyzed the role of DCIR–NA2 interaction in DC activation during DC-mediated T cell activation. For this, we exploited 2D2 TCR transgenic mice (2D2 mice) that express T cell receptors specific for a myelin oligodendrocyte glycoprotein amino acid 35–55 peptide (pMOG). Splenic DCs purified from WT or $Dcir^{-/-}$ mice were co-cultured with Thy1.2-positive T cells from 2D2 mice in the presence of pMOG, and gene expression was analyzed by RNA sequencing (RNA-seq). We found that the expression of 460 genes in the $Dcir^{-/-}$ DC-2D2 T cell co-culture was significantly higher than that in the WT DC-2D2 T cell co-culture (Fig. 7 c). To understand the functional features of these genes, a gene ontology (GO) analysis was performed. Interestingly, the gene sets associated with antigen presentation (*H2-Aa*, *Cd80*, *Cd86*, and *Cd40*) were significantly higher in the $Dcir^{-/-}$ DC co-culture, suggesting that DCIR-mediated inhibitory signal regulates antigen-presenting activity of DCs (Fig. 7 c).

We also found that the expression of cytokines such as *Il1a*, *Il1b*, *Il21*, and *Il1f9* and chemokines such as *Cxcl3*, *Cxcl2*, and *Ccl2* in 2D2 T cell–DC co-culture was highly augmented in $Dcir^{-/-}$ DCs (Fig. 7 d). In addition, the expression of other genes was also augmented, such as those associated with pattern recognition receptor signaling pathway (*Lyn*, *Tlr7*, *Ly96*, and *Hck*), protein phosphorylation (*Cd40*, *Tnfsf11a*, and *CD36*), cell migration
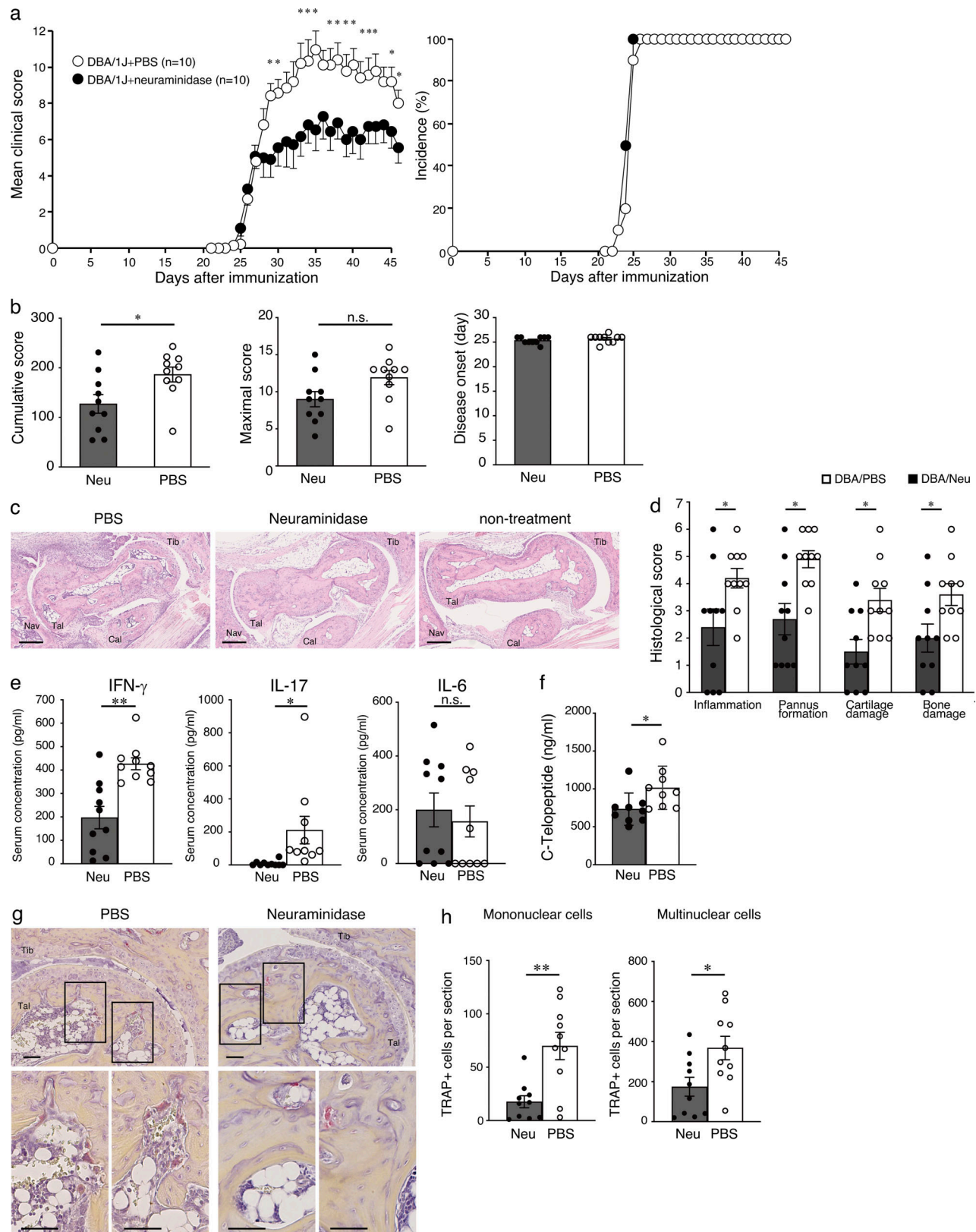
Figure 4. **Neuraminidase treatment ameliorates CIA in DBA/1J mice. (a)** Arthritic score and incidence of arthritis in DBA/1J mice after induction of CIA were analyzed with or without neuraminidase (Neu) treatment. Neuraminidase (0.1 U/mouse; Roche) was intravenously administered every 2 d before collagen immunization and six times every 2 d after immunization. Neuraminidase injected group: *n* = 10, PBS-injected group: *n* = 10. **(b)** Average cumulative clinical score, mean maximal score, and disease onset time are shown for each group. The P value of mean maximal score is 0.054. The bars show the mean ± SEM. **(c)** Sections (4 μm) of hind limb joints at day 40 after immunization were stained with H&E. Representative pictures are shown. Scale bar, 250 μm.

Neuraminidase-injected group: n = 10, PBS-injected group: n = 10. **(d)** Severity scores of inflammation, pannus formation, cartilage damage, and bone damage were assessed by histological examination of the H&E-stained sections (each section of right and left hind limbs was evaluated, and the total point of each parameter per mouse is six points). The bars show the mean ± SEM. The severity scores were evaluated from the sections of one CIA experiment. **(e and f)** Serum concentration of IFN-γ, IL-17, IL-6, and CTX-I was determined by ELISA. Sera were collected from neuraminidase- and PBS-treated mice at day 45 after immunization. The bars show the mean ± SEM. For cytokine detection, neuraminidase-injected group: n = 10, PBS-injected group: n = 10 (e). For CTX-I detection, neuraminidase-injected group: n = 9, PBS-injected group: n = 9 (f). **(g)** TRAP staining of hind limb joints at day 40 after immunization. Scale bar, 50 μm. n = 10 (neuraminidase), n = 10 (PBS). **(h)** The number of TRAP⁺ cells was counted in paw sections of neuraminidase- and PBS-treated DBA/1J mice. n = 10 (neuraminidase), n = 10 (PBS). The bars show the mean ± SEM. Statistical significances (*, $P < 0.05$; **, $P < 0.01$) are evaluated by Mann–Whitney U test (a), one-way ANOVA with Dunnett's post hoc test (b and d), and the two-tailed unpaired Student's t test (e, f, and h). Tal, talus; Cal, calcaneus; Tib, tibia; Nav, navicular.

(*Slamf8*, *Pla2g7*, and *Myo1f*), and transcription factors (*Aim4*, *Tnfaip3*, and *Acod1*).

Because the expression of genes involved in antigen presentation was augmented, we next analyzed the expression of these molecules on CD11c⁺ cells in the DC-2D2 T cell coculture by FACS. The expression of CD86 was reduced in neuraminidase-treated DCs cocultured with 2D2 T cells for 3 d in the presence of pMOG (Fig. 7 e). In this culture, the proportion of WT CD11c⁺ cells and the frequency of I-A/I-E⁺, CD86⁺, CD80⁺, and Ki67⁺ cells in CD11c⁺ cells were also significantly decreased after neuraminidase treatment compared with those in nontreated cells (Fig. 7 f). It should be noted, however, that the expression of these molecules was not affected by neuraminidase treatment in *Dcir⁻/⁻* DCs.

Since a set of genes related to antigen presentation was augmented in *Dcir⁻/⁻* DC-2D2 T cell co-culture, we examined antigen-presenting ability of WT and *Dcir⁻/⁻* DCs with or without neuraminidase treatment. Splenic DCs purified from WT or *Dcir⁻/⁻* mice were co-cultured with 2D2 T cells in the presence of pMOG, and the effects of neuraminidase treatment on T cell proliferation and cytokine production were examined. The extent of T cell proliferation in the presence of neuraminidase was lower in the co-culture with WT DCs than that in the absence of neuraminidase (Fig. 7 g). In contrast, neuraminidase treatment did not affect T cell proliferation with *Dcir⁻/⁻* DCs. Moreover, neuraminidase treatment resulted in a decrease in cytokine expression, such as GM-CSF, IFN-γ, and TNF-α, but not IL-17, and Ki67 expression in T cells in the co-culture with WT DCs (Fig. 7 h; and Fig. S4). However, neuraminidase treatment did not affect a cytokine-positive T cell population in *Dcir⁻/⁻* DC co-culture. We further examined the effect of NA2 on antigen-presenting ability of WT and *Dcir⁻/⁻* DCs. Consistent with the observation of neuraminidase treatment in WT DC-WT T cell co-culture, NA2 decreased the expression of cytokines, such as GM-CSF, IFN-γ, and TNF-α, but not IL-17, and Ki67 in T cells (Fig. 7 i). NA2 treatment in *Dcir⁻/⁻* DC-WT T cell co-culture had no effect on cytokine-positive T cell population (Fig. 7 i).

Finally, we activated 2D2 T cells with anti-CD3 and anti-CD28 antibodies in the presence of neuraminidase to examine the direct effects of neuraminidase on T cells. As shown in Fig. S5, a and b, cytokine-positive T cells and cytokine concentrations in the culture supernatants were comparable irrespective of neuraminidase treatment. These results indicate that T cell activation is suppressed indirectly through interaction with DCs, suggesting that NA2-induced DCIR stimulation suppresses the antigen-presenting ability of DCs.

Discussion

In this report, we have identified NA2 as an endogenous functional ligand for DCIR. DCIR expressed on osteoclasts and DCs binds NA2 on macrophages, osteoclasts, osteoblasts, and DCs in a CRD- and Ca²⁺-dependent manner. The treatment of WT BMCs, but not of *Dcir⁻/⁻* BMCs, with NA2 suppressed the differentiation of osteoclasts, indicating that NA2 is a functional ligand for DCIR. Furthermore, BMCs from *Dcir⁻/⁻* mice differentiated more efficiently into osteoclasts than WT BMCs upon stimulation with M-CSF and RANKL, suggesting that NA2 on BMMs regulates their differentiation into osteoclasts. Interestingly, neuraminidase treatment, which forces an increase in NA2 exposure on the cell surface by removing the terminal sialic acids of N-glycans, suppressed the RANKL-induced osteoclastogenesis of BMMs. Since neuraminidase treatment had no observable effect in *Dcir⁻/⁻* osteoclasts, it is reasonable to assume that the suppression was mediated by DCIR. These data suggest that a large proportion of NA2 is masked by sialic acids under physiological conditions and becomes available after neuraminidase treatment. Human DCIR also binds NA2 in a Ca²⁺-dependent manner, and NA2 suppressed human CD14⁺ cell differentiation into osteoclasts. We do not know yet whether this interaction of NA2 with DCIR occurs in cis, trans, or both manners on BMMs.

Consistent with our observation, it was reported that human DCIR binds biantennary N-glycans (Hsu et al., 2009), and GlcNAcβ1-2Man of biantennary N-glycans are the main epitope for the binding (Nagae et al., 2016). Although the binding of DCIR to fucose, mannose, sulfated LacNAc, Lac, Lewisᵇ, and Man₃ was reported using DCIR-Fc (Bloem et al., 2013; Hsu et al., 2009; Lee et al., 2011), we could not reproduce the results, probably because the binding affinity was too low (Fig. S2). We were not able to test for the binding to Man₃ because the glycanarray we used did not include Man₃. However, none of these molecules was shown to induce the ITIM-mediated biological function of DCIR.

In support of our conclusion that NA2 is a ligand for DCIR, the binding of DCIR-Fc to 293T cells was enhanced by the expression of Mgat2, which catalyzes biantennary N-glycan synthesis, and is inhibited by tunicamycin, a N-glycan synthesis inhibitor, but not by the O-glycan synthesis inhibitor benzyl-α-GalNAc. Furthermore, the cytidine 5′-monophosphate–sialic acid transporter–deficient Lec2 cells showed higher levels of DCIR-Fc binding, and uridine 5′-diphosphate–galactose–transporter–deficient *Lec8* cells did not bind DCIR-Fc.

We showed that the development of CIA and EAE was suppressed by treatment with neuraminidase in WT mice, but not
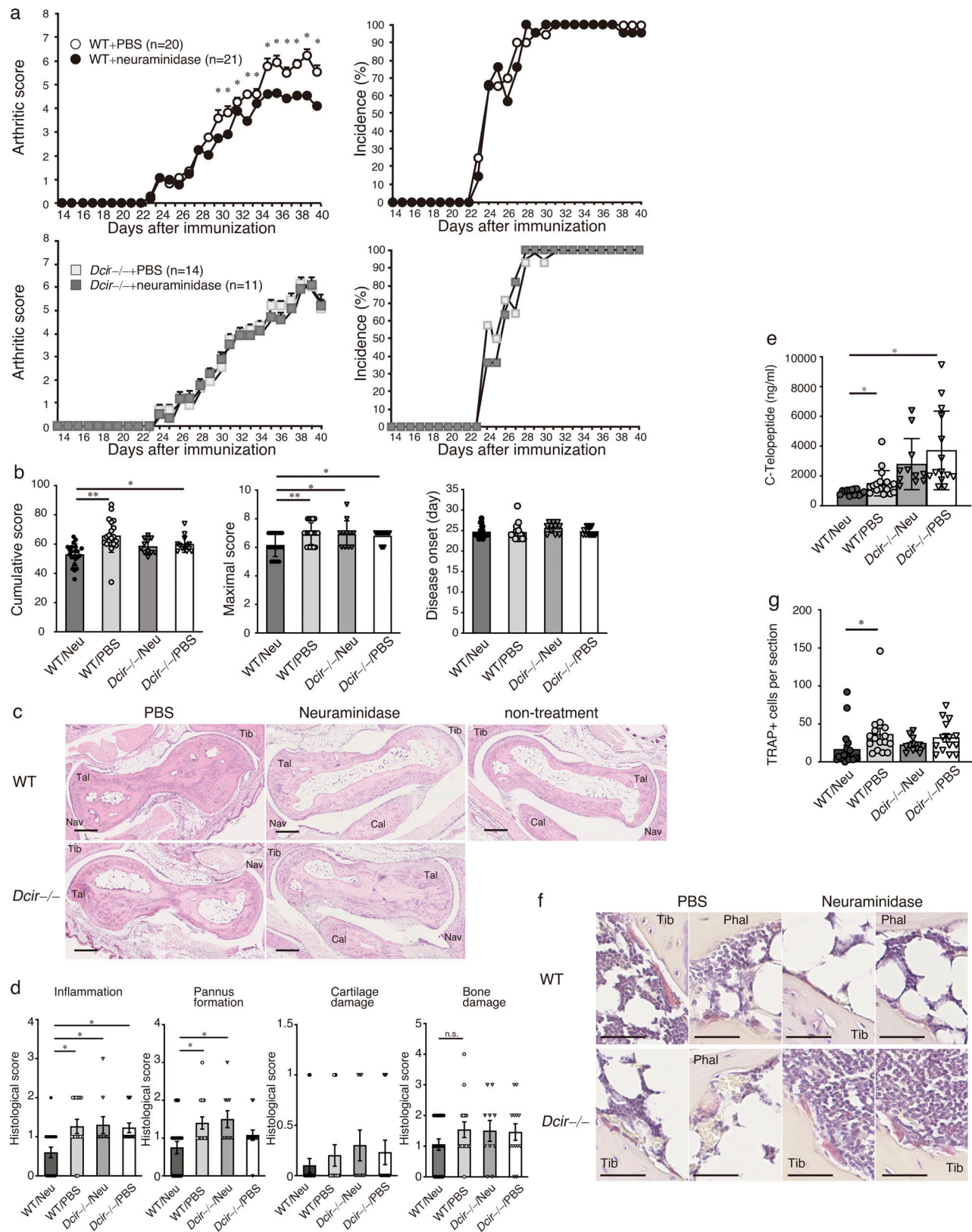
Figure 5. **Intravenous administration of neuraminidase suppresses the development of CIA. (a)** The clinical score and incidence of arthritis after induction of CIA was analyzed with and without neuraminidase (Neu) treatment. WT mice (top) or $Dcir^{-/-}$ mice (bottom) were intravenously administered with neuraminidase (2 U/mouse, NEB) or PBS 1 d before immunization and a further six times every other day after immunization. WT mice, PBS: $n = 20$, neuraminidase: $n = 21$; $Dcir^{-/-}$ mice, PBS: $n = 14$, neuraminidase: $n = 11$. The data are representative of two independent experiments. **(b)** Disease parameters. Average cumulative clinical score, mean maximal score, and disease onset time are shown for each group. **(c)** Representative histological images of the joints of

hind limbs. The sections of joints at day 45 after collagen immunization were stained with H&E. Scale bar, 500 µm. Tal, talus; Cal, calcaneus; Tib, tibia; Nav, navicular. **(d)** Histological severity scores. Inflammation, pannus formation, cartilage damage, and bone damage were assessed by the H&E sections of the right and left hind limbs (the full score of each parameter per mouse is six points). The bars show the mean ± SD. *, P < 0.05; **, P < 0.01; Mann–Whitney U test (a) and one-way ANOVA with Dunnett's post hoc test (b and d). **(e)** Serum concentration of CTX-I was determined by ELISA. Sera were collected from neuraminidase- and PBS-treated mice at day 40 after immunization. WT mice, PBS: n = 18, neuraminidase: n = 16; Dcir⁻/⁻ mice, PBS: n = 14, neuraminidase: n = 11. The data are representative of two independent experiments. The bars show the mean ± SEM. Statistical analysis was performed using one-way ANOVA with Dunnett's post hoc test. **(f)** Representative TRAP staining images of paw sections from neuraminidase- and PBS-treated mice. The sections of joints at day 40 after collagen immunization were stained with TRAP. Scale bar, 50 µm. Phal, phalange. **(g)** TRAP⁺ cells were quantified in paw sections of the right and left hind limbs. WT mice, PBS: n = 16, neuraminidase: n = 20; Dcir⁻/⁻ mice, PBS: n = 14, neuraminidase: n = 11. The bars show the mean ± SEM. *, P < 0.05; one-way ANOVA with Dunnett's post hoc test. Data (c, d, f, and g) were evaluated from one CIA experiment.

---

in *Dcir⁻/⁻* mice, suggesting that excess exposure of NA2 suppresses the development of these diseases in a DCIR-dependent manner. These results are consistent with our previous observations that the development of CIA and EAE is exacerbated in *Dcir⁻/⁻* mice (Fujikado et al., 2008; Seno et al., 2015), although in the present experiments, exacerbation of CIA and EAE in *Dcir⁻/⁻* mice was not observed. This is because we used more severe disease induction conditions than those used in the previous experiments in order to see suppressive effects of neuraminidase more clearly, and the disease severity scores were saturated even in WT mice.

Then we investigated the mechanism of how DCIR signaling regulates development of CIA and EAE. We found by RNA-seq analysis that the expression of several groups of genes was augmented in *Dcir⁻/⁻* DCs co-cultured with pMOG-specific 2D2 T cells in the presence of pMOG. One of these groups was categorized as the genes involved in antigen presentation, including the *H2-Aa*, *Cd80*, *Cd86*, and *Cd40* genes. Among them, the major histocompatibility complex H2 is important for antigen presentation, and CD80 and CD86 are important coreceptors for T cell activation. CD40 signaling in DCs induces cytokine production, such as IL-1β and TNF, and promotes antigen presentation through activation of the TRAF–NF-κB and/or MAPK pathways (Ma and Clark, 2009). Thus, these results show that NA2-induced DCIR signaling suppresses antigen presentation by DCs.

The RNA-seq analysis also revealed that the expression of gene sets relating to pattern recognition receptor signaling pathways (*Lyn*, *Tlr7*, *Ly96*, and *Hck*), protein phosphorylation (*Cd40*, *Tnfsf11a*, and *CD36*), cell migration (*Slamf8*, *Pla2g7*, and *Myo1f*), and transcription (*Tnfaip3*, *A20*, *Acod1*, and *Id1*) were also activated in *Dcir⁻/⁻* mice. Thus, these observations indicate that not only the genes involved in antigen presentation but also a broad range of gene expression are augmented in *Dcir⁻/⁻* DC and T cell co-culture, probably reflecting an excessively activated state of DCs.

In support of the RNA-seq results, we found by FACS analysis that the expression of molecules involved in antigen presentation of DCs was reduced in neuraminidase-treated DCs cocultured with 2D2 T cells. 2D2 T cell proliferation in the presence of pMOG and WT DCs, but not *Dcir⁻/⁻* DCs, was suppressed by treatment with neuraminidase. Cytokine production from 2D2 T cells upon incubation with pMOG and DCs was also suppressed by neuraminidase treatment. These results indicate that antigen-presenting activity of DCs is regulated by the DCIR-NA2 interaction. Therefore, we conclude that the development of CIA and EAE is suppressed by the treatment with neuraminidase,

because antigen presentation by DCs is reduced. Although the content of NA2 is likely to be regulated by the balance between sialyltransferases and neuraminidases, the detailed regulatory mechanisms have yet to be elucidated. While the inhibitory effect of neuraminidase treatment on in vitro RANKL-induced osteoclast formation was reported by Takahata et al. (2007), the molecular mechanism was not elucidated.

DCIR-dependent amelioration of CIA and EAE by the treatment with neuraminidase was rather unexpected for us, because sialic acids decorating the terminus of carbohydrate chains on glycoproteins and glycolipids are among the most important signaling molecules and are recognized by many receptors. For example, Siglec family members are known to be the receptors for sialic acids (Crocker et al., 2007). The expression of Siglec-15 is up-regulated during RANKL-induced osteoclastogenesis and facilitates osteoclast differentiation (Kameda et al., 2013). Deficient mice for Siglec-2 show reduced mature B cells and thymus-independent B cell responses (Nitschke, 2005). Siglec-F–deficient mice show enhanced eosinophilia in allergic airway inflammation (Zhang et al., 2007), and B1a cells are increased in Siglec-G–deficient mice (Hoffmann et al., 2007). The selectin family members are another category of receptors whose activities are regulated by the sialylation of the ligands. Leukocyte rolling, neutrophil recruitment into the inflamed peritoneal cavity, and lymphocyte homing to secondary lymphoid organs are impaired in mice lacking two sialyltransferases (St3gal4/St3gal6), which are important for the synthesis of E- and P-selectin ligands (Yang et al., 2012). The activity of other lectins that recognize terminal Gal, such as galectins (Thiemann and Baum, 2016), may also be affected by the neuraminidase treatment. Nonetheless, we observed only marginal effects, if any, on other lectins, which were considered likely to be affected by the treatment with neuraminidase. These observations suggest that DCIR is of primary importance among the C-type lectins and other lectins for the regulation of the immune system and bone metabolism under our experimental conditions.

To conclude, we have shown that NA2 is a functional ligand for DCIR, and its activity is regulated by the modification of the terminal sialic acids to regulate DC maturation and osteoclastogenesis. However, it still remains to be elucidated where and how the terminal sialic acid content of N-glycans is regulated. In addition, the roles of the DCIR-NA2 axis in humans also remain to be elucidated, although we found that NA2 regulates human osteoclast differentiation in vitro. The findings of this study have potential for use in the development of new therapeutics for the treatment of immune and bone metabolic diseases.
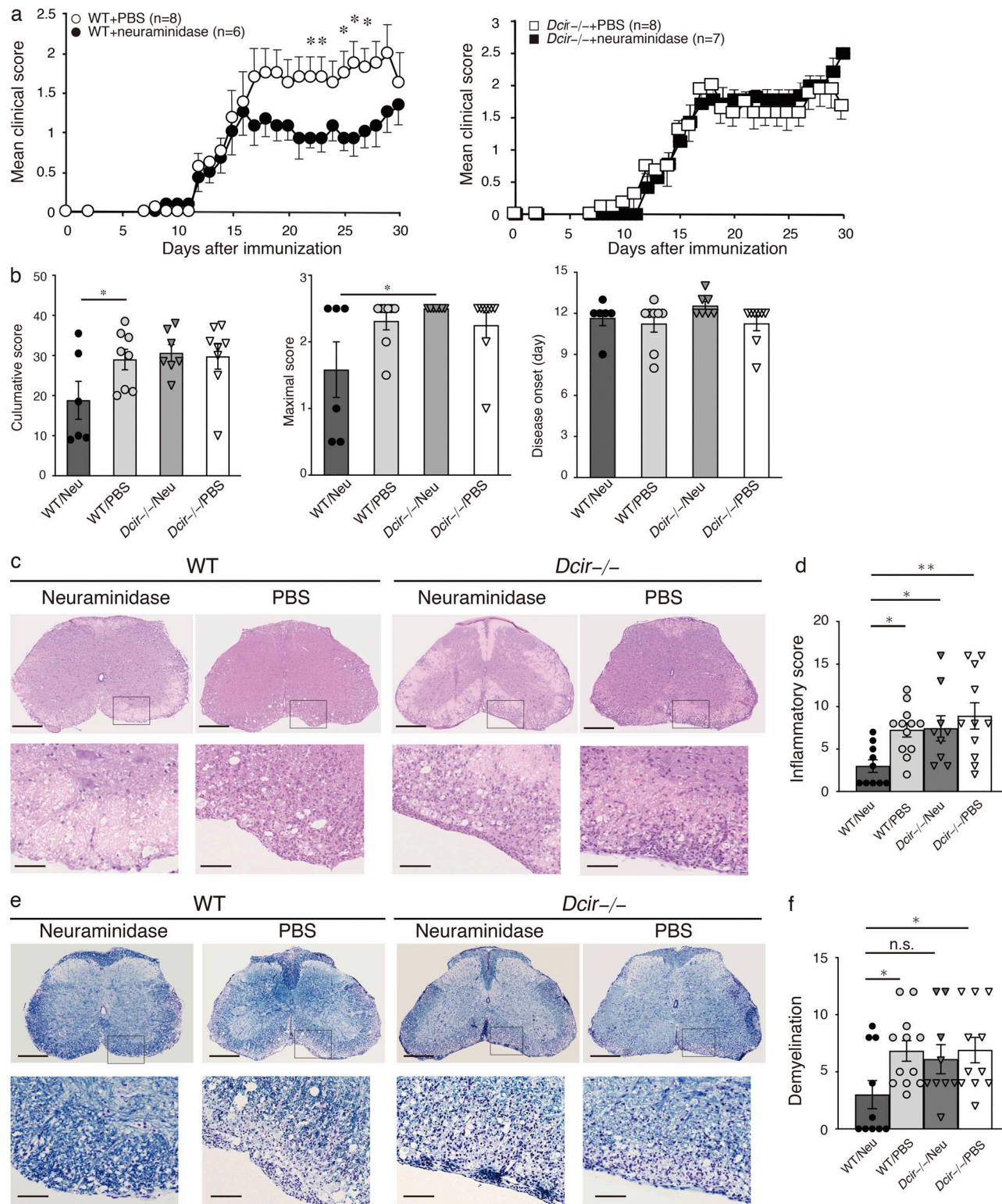
Figure 6. **Intravenous injection of neuraminidase suppresses the development of EAE. (a)** WT and $Dcir^{-/-}$ mice were intravenously administered with neuraminidase (Neu; 0.1 U/mouse, Roche) 6 d before pMOG immunization and seven times every 2 d after immunization. Then the development of EAE was inspected every day after the induction of EAE. Neuraminidase (WT, n = 6; $Dcir^{-/-}$, n = 7) or PBS (WT, n = 8; $Dcir^{-/-}$, n = 8). The data are representative of two independent experiments. The bars show the mean ± SD. *, P < 0.05; **, P < 0.01 (Mann–Whitney U test). **(b)** Disease parameters, including average cumulative clinical score, mean maximal score, and disease onset time are shown for each group. The bars show the mean ± SEM. *, P < 0.05 (one-way ANOVA with Dunnett's post hoc test). **(c and d)** The sections of spinal cords at day 30 after immunization were stained with H&E or KB in neuraminidase-treated or PBS-treated mice. Representative pictures are shown. Scale bar, 250 μm in low-power fields and 50 μm in high-power fields. Neuraminidase (WT, n = 10; $Dcir^{-/-}$, n = 10) or PBS (WT, n = 12; $Dcir^{-/-}$, n = 11). **(e and f)** Severity scores of inflammation and demyelination were assessed by histological examination of the H&E or KB stained sections (three sections of spinal cord per mouse were evaluated). The bars show the mean ± SEM. Neuraminidase (WT, n = 10; $Dcir^{-/-}$, n = 10) or PBS (WT, n = 12; $Dcir^{-/-}$, n = 11). Statistical significances (*, P < 0.05; **, P < 0.01) are evaluated by one-way ANOVA with Dunnett's post hoc test (d and f). The severity scores were evaluated from one EAE experiment.

Kaifu et al.
The DCIR-NA2 in the immune and bone system

Journal of Experimental Medicine   12 of 20
https://doi.org/10.1084/jem.20210435

Materials and methods

Mice

$Dcir^{-/-}$ mice were generated as described (Fujikado et al., 2008), and these mice were backcrossed to C57BL/6J for 12 generations. 2D2 TCR transgenic (2D2 Tg) mice were purchased from The Jackson Laboratory. All the mice used in these experiments were 8–12 wk old, and these age- and sex-matched control C57BL/6J and DBA/1J mice were purchased from Japan SLC, Inc. All the mice were housed in specific pathogen–free animal rooms of the Research Institute for Biomedical Sciences, Tokyo University of Science, and the Tohoku Medical and Pharmaceutical University. Animal experiments were performed following the guidelines of each university and were approved by the Animal Experimental Committee of the Tokyo University of Science and the Animal Experiments Committee of Tohoku Medical and Pharmaceutical University.

Cell culture

HEK293T, CHO cells, and CHO mutants with defective glycosyltransferases (Lec1, Lec2, and Lec8, kindly provided by J. Hirabayashi; Stanley et al., 1975) were cultured in DMEM (Gibco, Life Technologies) containing penicillin (100 U/ml), streptomycin (100 µg/ml), and 10% heat-immobilized FBS.

In vitro culture of BM-derived macrophages and osteoclasts

To differentiate BM-derived macrophages, BMCs were isolated by flushing the BM cavity of femurs with an α-MEM (Gibco, Life Technologies) supplemented with penicillin (100 U/ml), streptomycin (100 µg/ml), and 10% heat-inactivated FBS. Red blood cells were destroyed in a hemolysis buffer (consisting of 140 mM NH_4Cl and 17 mM Tris-HCl, pH 7.2) for 10 min on ice, and the treated cells were preincubated in a 100-mm dish for 1 h. The nonadherent cells (hematopoietic cells) were harvested and seeded at 50,000 cells per well in 96-well plates in the presence of 20 ng/ml of recombinant human M-CSF (R&D Systems, Inc.) for 2 d. The cells proliferated in response to M-CSF are defined as BMMs in this paper. To generate osteoclasts, the BMMs were further cultured in the presence of 20 ng/ml of M-CSF and 100 ng/ml of human recombinant soluble RANKL (Oriental Yeast Co., Ltd.), with the culture medium changed every 2 d. To maturate macrophages, BMMs were incubated in 20 ng/ml of M-CSF for 6 d with the medium changed every 2 d.

Measurement of osteoclast formation by TRAP staining

Adherent cells were fixed in 10% formalin for 3 min, followed by further fixation in a fixative buffer consisting of 50% ethanol and 50% acetone for 1 min. The cells were stained with Naphthol AS-MX phosphate (Nacalaitesque) and Fast-Red (Nacalaitesque) for 10–15 min at room temperature and washed with water three times. TRAP-positive cells with >3 or 10 nuclei were counted as multinucleated osteoclasts.

Human osteoclast formation

CD14+ cells from human peripheral blood were purchased from Lonza. These cells were seeded at 100,000 cells per well in a 96-well plate (Iwaki) and cultured in the presence of recombinant human M-CSF (30 ng/ml; PeproTech) and sRANKL (100 ng/ml)

with 1 µg/ml of BSA or NA2-BSA for 8 d. The culture medium was changed every 2 d. These cells were stained with Naphthol AS-MX phosphate and Fast-Red, and TRAP+ cells with >50 µm diameter were counted as osteoclasts.

Retroviral infection to BMCs

Murine DCIR cDNA was amplified using the following primers: sense 5′-CGGGATCCCACCATGGCTTCAGAAATCACTTATG-3′ and antisense 5′-CGGAATTCTCATAAGTTTATTTTCTTCA-3′. The PCR product was cloned into pMXs-IRES-Puro (kindly provided by T. Kitamura, The University of Tokyo, Tokyo, Japan) via the BamHI and EcoRI sites. The pMXs vector was amplified in Escherichia coli (DH5α). DCIR Y/F mutation was generated using a KOD-Plus-Mutagenesis Kit (TOYOBO). In brief, to replace the tyrosine in the ITIM of DCIR to phenylalanine, we designed a forward primer 5′-CACTtTTGCAGAAGT GAAGTTCAAGAATGAATC-3′ (adenosine was changed into lowercase T) and a reverse primer 5′-ATTTCTGAAGCCATGGTG GGATCCTTGGTTAAC-3′. The inverse PCR was performed using the pMXs vector as a template, which was digested by Dpn I capable of digesting methylated DNA from typical E. coli cell lines. Non-digested PCR products were self-ligated by T4 polynucleotide kinase and ligase at 16°C for 1 h. A Plat-E packaging cell line (provided by T. Kitamura) was cultured in 10% FBS α-MEM and split every second day at a ratio of 1:5. The retroviral vectors were transfected in Plat-E cells by Lipofectamine 2000 (Invitrogen). After 8 h of incubation, the medium was changed and further incubated for 24 h. The retroviral supernatant was collected and frozen at –80°C until it was used. To retrovirally transduce DCIR and DCIR mutant BMs, nonadherent BMCs were cultured in 100 µl of medium containing 20 µl of retroviral supernatant, and the medium was replaced every 2 d.

FACS analysis

BMCs underwent blood cell lysis with a hemolysis buffer (consisting of 140 mM NH_4Cl and 17 mM Tris-HCl, pH 7.2) on ice. The BMMs and osteoclasts were detached and washed with a FACS buffer consisting of 2% FBS in PBS to remove serum components. The Fc receptors on these cells were blocked with 2.4G2, an Fc receptor blocker, at 4°C for 10 min. These cells were washed twice with a FACS buffer and incubated with fluorescence-conjugated antibodies for 30 min on ice. Commercially available antibodies are listed in Table S1.

To detect the DCIR ligand, 10 µg/ml of DCIR-Fc-protein, mutated DCIR-Fc-protein, or Fc-protein were preincubated with 5 µg/ml of FITC-conjugated anti-human IgG (Jackson ImmunoResearch Laboratories, Inc.) in a TSA buffer containing 2 mM calcium chloride, 2 mM magnesium chloride, and 0.5% BSA in Tris-buffered saline for 15 min at room temperature. Macrophages and osteoclasts were stained with the protein complex for 1 h at 4°C, followed by gentle washing with the TSA buffer. Flow cytometry was performed on FACSCanto II (Becton Dickinson) or Attune NxT flow cytometer (Thermo Fisher Scientific) and analyzed using FlowJo software (Tree Star, Inc.).

For intracellular cytokine staining, cells were first stained with antibodies against cell surface markers. The cells were fixed and permeabilized using an intracellular fixation and
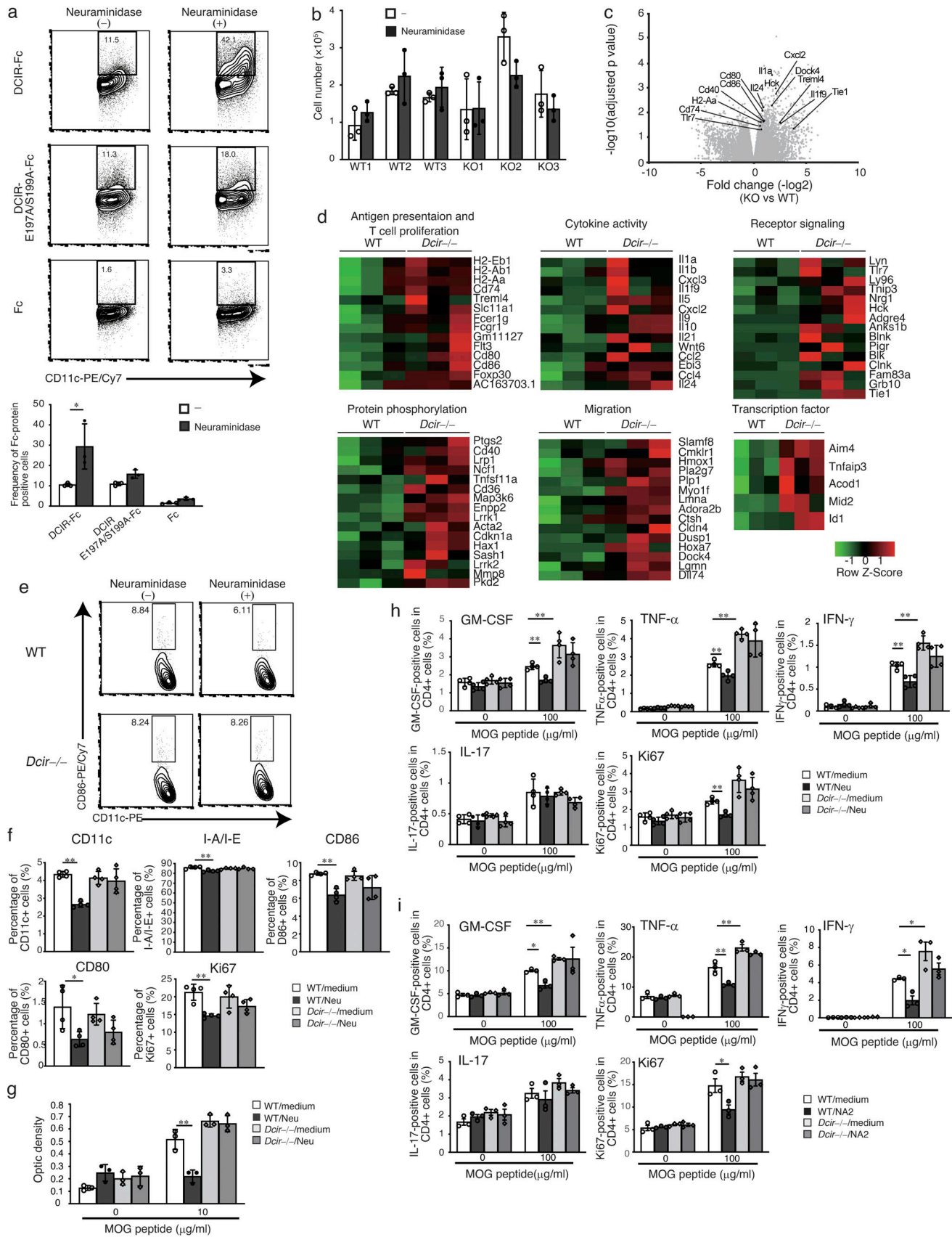
Figure 7. Neuraminidase treatment reduces antigen-presenting ability of DCs in a DCIR-dependent manner. (a) DCIR-Fc binding to GM-DCs after neuraminidase (Neu) treatment. GM-DCs were differentiated for 10 d in culture, and 1 × 10⁶ GM-DCs were treated with neuraminidase (0.1 U/ml; Roche) for

30 min before the binding assay. **(b)** WT and *Dcir*$^{-/-}$ BMCs were induced to differentiate with GM-CSF. Neuraminidase (1 mU/ml; Roche) was added at day 0 and three times every 2 d, and cell numbers were counted at day 8. **(c)** Changes in gene expression in the co-culture of 2D2 T cells and DCs with pMOG (100 µg/ml) were examined between WT (*n* = 3) and *Dcir*$^{-/-}$ DCs (*n* = 3), and −log 10 P value versus log2 fold-change are plotted on the y and x axes, respectively. Genes with high fold-change are labeled. **(d)** Heatmap of changes in gene expression between WT (*n* = 3) and *Dcir*$^{-/-}$ DCs (*n* = 3) in 2D2 T cell and DC co-cultures with pMOG (100 µg/ml). Gene sets of indicated categories are presented in color scale. **(e and f)** The expression of DC maturation and proliferation markers in CD11c$^+$ cells in the co-culture of DCs and 2D2 T cells in the presence of pMOG (100 µg/ml). MACS-sorted splenic DCs of WT or *Dcir*$^{-/-}$ mice were cocultured with Thy1.2$^+$ T cells from 2D2 Tg mice in the presence or absence of neuraminidase (0.1 mU/ml; Roche, added at days 1 and 2). Cells were stained at day 3 with anti-CD11c, anti–I-A/I-E, anti-CD80, anti-CD86, and anti-Ki67 antibodies, and expression on CD11c$^+$ cells was analyzed by FACS. The data are representative of two independent experiments. **(g)** T cells (Thy1.2$^+$) from 2D2 Tg mice, co-cultured with either WT or *Dcir*$^{-/-}$ DCs in the presence of pMOG (10 µg/ml), were treated with neuraminidase (0.01 mU/ml; Roche) for 3 d, followed by BrdU incorporation for 6 h. Then, incorporated BrdU was detected by colorimetric immunoassay. Data are the mean ± SD of triplicate cultures. The data are representative of two independent experiments. **(h)** Cytokine expression in 2D2 T cells co-cultured with either WT or *Dcir*$^{-/-}$ DCs in the presence or absence of neuraminidase (0.1 mU/ml; Roche) was analyzed by FACS after 3 d in culture. Cytokine-positive 2D2 T cells (GM-CSF, IFN-γ, TNF-α, and IL-17) and proliferation marker–positive cells (Ki67) were determined with a flow cytometer. CD4$^+$ T cells were gated from the CD3$^+$ cell population. Data are the mean ± SEM of triplicate cultures. The data are representative of two independent experiments. **(i)** Cytokine expression in 2D2 T cells co-cultured either with WT or *Dcir*$^{-/-}$ DCs in the presence or absence of NA2-BSA (2 µg/ml). Data are the mean ± SEM of triplicate cultures. The data are representative of two independent experiments. *, P < 0.05; **, P < 0.01; one-way ANOVA with Dunnett's post hoc test (f–i).

permeabilization buffer set (eBioscience) and then stained for intracellular cytokines, such as IFN-γ, IL-17, TNF-α, GM-CSF, and Ki67.

Quantitative RT-PCR and conventional PCR

Total RNA was extracted from BMMs and osteoclasts using the GenEluteTM Mammalian Total RNA Miniprep kit (Sigma-Aldrich). Quantification of total RNA was performed using Nano-Drop. 1 µg of total RNA was reverse-transcribed using Superscript II Reverse transcription (Invitrogen) to synthesize first cDNA. The quantitative PCR was performed in a total reaction volume of 10 µl including 5 ng equivalent to total RNA, SYBR Green I (Takara Bio), and a set of forward and reverse primers (Operon) in duplicate or triplicate samples. Quantification was performed on CFX384 Real-Time system (Bio-Rad Laboratories, Inc.). Cycling program was 1 cycle of 95°C for 1 min, followed by 44 cycles of a set of 95°C for 3 s and 60°C for 30 s. The primer sets used to detect each transcript in macrophages or osteoclasts are described in Table S2. The final concentration of the primers was 400 nM. GAPDH was used as an internal housekeeping gene control. The target genes and the housekeeping gene were quantified simultaneously in one plate, with water samples as the negative reference. The difference in RNA quality and initial quantity of samples was normalized to GAPDH. The relative expression of the targeted gene ($2^{-\Delta\Delta Ct}$ method) was calculated from the following equation: $2^{-\Delta Ct}$, where ΔCt = average Ct for the gene of interest – average Ct for the housekeeping gene. The fold change of a targeted gene on days 3 and 4 relative to a sample on day 2 was determined by the following: $2^{-\Delta\Delta Ct}$, where $\Delta\Delta Ct$ = (average Ct for gene of interest – average Ct for the gene of a housekeeping gene) each sample on days 3 and 4 – (average Ct for gene of interest – average Ct for the housekeeping gene) sample on day 2. The SD was calculated according to the mathematical method described in earlier reports (Bookout and Mangelsdorf, 2003; Livak and Schmittgen, 2001).

We performed RT-PCR in 20 µl of reaction volume with Extaq (Takara Bio). A primer set for amplifying DCIR was sense 5′-CATTTCCCTTATCTCGCCCTGG-3′ and anti-sense 5′-GCATGAGTGTCCAAGATCC-3′, which amplified a 686-bp product. The PCR reaction was run in the following program: 30 cycles of 98°C for 10 s, 55°C for 30 s, and 72°C for 1 min. GAPDH was used as an internal control.

Generation of Fc-fused DCIR protein

Murine DCIR cDNA covering EC from 70 to 238 at the amino acid level was subcloned into pFUSE-hIgG2-Fc2 vector (Invivogen) at the *Bgl* II site. cDNA coding the EC was generated with a primer set: sense 5′-ATAAGATCTCAAAAGTACTCTCAACTTCTT-3′ and anti-sense 5′-ATAAGATCTTAAGTTTATTTTCTTCATC-3′. Site-directed mutations of the CRD domain in which glutamic acid and serine were replaced with alanine were established by KOD-Plus-Mutagenesis Kit (TOYOBO) according to the manufacturer's instructions. The primer set for the mutagenesis is as follows: sense 5′-GGTGCTCCCGCTAGTGGCAATGAAAAA TGTGCT-3′ and anti-sense 5′-TAGTGTAAGACCGTGTTACCA CGAGGGGCGATCA-3′. The sequences encoding human DCIR EC (70–237 amino acids) were amplified by PCR with a primer set (sense 5′-ATACCATGGGTCAAAAATATTCTCAGCTTCTT-3′ and anti-sense 5′-ATAAGATCTTAAGTGGATCTTCATCATC-3′). The resulting PCR fragment was ligated into a pFUSE-hIgG2-Fc2 vector (Invivogen) via *Nco*I and *Bgl*II. We generated three plasmid vectors for DCIR-Fc (the EC of mDCIR), mutant DCIR-Fc (inactive form of CRD domain, E197A/S199A), and Fc-protein (constant region of Ig). We transfected the plasmids into HEK293T cells by Lipofectamine LTX (Invitrogen), followed by incubation in Opti-MEM (Invitrogen) including 2% low IgG FBS (Invitrogen) for 15 d with medium change every 3 d. The Fc-chimeric proteins were purified from collected supernatant by affinity chromatography on Protein A-Sepharose (GE Healthcare).

Generation of Mgat2-293T cells

Murine GnT-II (*Mgat2*) cDNA from osteoblasts were inserted into pcDNA3.1(+)/FLAG vector (Invitrogen) at *Bam*HI and *Eco*RI sites. The cDNA was synthesized with a primer set: *Bam*H1, 5′-ATAGGA TCCATGAGGTTCCGCATCTACAAACG-3′; *Eco*RI, 5′-ATAGAATTC CTGCAGTCTTCTATAACTTTTACAGAGTTCATGG-3′. We transfected the vector into HEK293T cells by Lipofectoamine LTX (Invitrogen) and incubated in Opti-MEM for 24 h. The transient Mgat2-293T cells were harvested with trypsin digestion and resuspended in a TSA buffer for the FACS analysis.

Functional assay of DCIR ligand

WT and *Dcir*$^{-/-}$ BMMs were induced to differentiate osteoclasts with M-CSF and RANKL, as described above. NA2–polyacrylamide

(PAA), purchased from GlycoTech, was applied at the beginning of the culture of nonadherent BMCs and consistently added each time the medium was replaced. The number of osteoclasts was determined by TRAP staining.

Co-culture of calvarial cells and nonadherent BMCs
Primary calvarial cells were enzymatically harvested and seeded at 200,000 cells/well in 12-well plates in α-MEM containing vitamin D3 (10^{-8} M) and prostaglandin E2 (10^{-6} M) for 24 h. A 10-fold number of nonadherent BMCs was co-cultured in the primary osteoblasts for 7 d, and the medium was changed every 3 d. In some experiments, neuraminidase or β-galactosidase (ProZyme Inc.) was applied in the co-culture system, and the enzymes were added at the time the medium was changed.

Tunicamycin, benzyl-α-GalNAc, and neuraminidase treatment
Primary osteoblasts cultured for 5 d were treated with either tunicamycin (Sigma-Aldrich; final concentration, 1 µg/ml) or benzyl-α-GalNAc (Sigma-Aldrich; final concentration, 2 mM) for 24 h at 37°C. The osteoblasts were harvested with trypsin and resuspended in a TSA buffer. The BM-derived macrophages for 6-d cultures were harvested using Cell Dissociation Solution Non-enzymatic 1× (Sigma-Aldrich) and resuspended in the TSA. The cells were treated with 5 mU neuraminidases (from *Arthrobacter* ureafacines; 10269611001; Roche; specific activity is ∼25 U/mg protein) consisting of a mixture of isoenzymes (L, M1, M2, and S) at 37°C for 30 min. These cells were washed with the TSA buffer and then subjected to an FACS analysis.

To measure the effect of the removal of sialic acid on osteoclastogenesis, osteoclasts were induced from nonadherent BMCs in the presence of 0.1 U/ml neuraminidase (Roche). Neuraminidase was replaced when the culture medium was changed every second day. In the co-culture system of osteoblasts with BMCs to induce osteoclasts, 0.1 U/ml of neuraminidase was presented at the start of the cell culture. Neuraminidase was replaced every 3 d.

Primary murine osteoblast culture
Calvarial cells were prepared by sequential digestion in accordance with the standard method. Briefly, calvaria from 1- to 2-d-old neonates were surgically isolated, and the adherent mesenchymal tissues were trimmed. The neonatal calvaria underwent a first digestion by a degrading solution containing 0.1% collagenase (Wako) and 0.1% dispase (Roche Diagnostics Japan) for 10 min at 37°C with agitation. The solution was discarded to remove debris, and the remaining calvaria were further digested by the same degrading solution for 1 h at 37°C. The cells isolated from the serial digestions were suspended in an α-MEM containing 10% FCS, penicillin (100 U/ml), and streptomycin (100 µg/ml), and plated at a concentration of 2×10^5 cells/well in 12-well plates. After 2 d in culture, the cells were incubated in an osteogenic medium (α-MEM supplemented with 10% FBS, 50 µg/ml ascorbic acid [Sigma-Aldrich], 10 mM β-glycerophosphate [Calbiochem], and antibiotics) for 14 d or 21 d, with the medium replaced every 3 d for the entire duration.

Preparation of OsteoMacs
Calvaria cells were obtained from newborn mice as described in the Materials and methods section. Red blood cells were lysed in a hemolysis buffer for 10 min at 37°C. The remaining cells were resuspended in 90 µl of autoMACS Running Buffer (Miltenyi Biotec Inc.) per 10^7 cells and incubated with 10 µl of CD11b MicroBeads (Miltenyi Biotec Inc.) per 10^7 cells for 15 min at 4°C. The cells were washed by autoMACS Running Buffer and resuspended up to 10^8 cells in 500 µl of autoMACS Running Buffer, and passed through a 75 nylon mesh (75 × 75 µm mesh) to remove cell clumps. CD11b-positive and -negative fractions were separated by an auto MACS Pro separator (Milteny Biotec Inc.), and these cells were used as OsteoMacs or primary osteoblast cells, respectively.

Glycan array assay
The glycan-protein interaction was detected in a glycan microarray with the evanescent-field fluorescence-assisted detection system developed by Tateno et al. (2008). Briefly, glycan probes, including glycoproteins and glycoside-PAA, were immobilized on microarray-grade epoxy-activated glass slides (Schott AG) in triplicate spots using a noncontact microarray printing robot, MicroSys 4000 (Genomic Solutions Inc.). The glass slides were incubated at 25°C for 3 h and washed with a reaction buffer consisting of 25 mM Tris–HCl, pH 7.4, containing 0.8% NaCl, 1% (vol/vol) Triton X-100, 1 mM $MnCl_2$, and 1 mM $CaCl_2$, to remove immobilized materials, followed by blocking in TBS (25 mM Tris-HCl, pH 7.4, with 0.8% NaCl and 1% BSA) at 20°C for 1 h. A protein complex of DCIR-Fc, mutant DCIR-Fc, or Fc with Cy3-labeled anti-human Fc antibodies was formed in a reaction buffer at room temperature for 20 min and kept in the dark. The protein complex was applied to a chamber of the glass slide at 100 µl per chamber and was incubated at 20°C for 3 h. Without washing, the binding was detected by an evanescent-field activated fluorescence scanner, SC-Profiler (Moritex), and the data were analyzed by the Array Pro analyzer Ver. 4.5 (Media Cybernetics, Inc.). Subtracted raw intensity from background intensity is net intensity, which is presented as the average ± SD of triplicate spots.

Human DCIR-Fc binding to NA2 BSA
NA2-BSA, which contains ∼15 NA2 molecules on a BSA molecule, or BSA (10 µg/ml in TBS consisting of 20 mM Tris and 150 mM NaCl, pH 7.4), were precoated on a 96-well plate at 4°C for overnight. Human DCIR-Fc proteins (5 µg/ml) in TBS containing 2 mM $CaCl_2$ and 2 mM $MgCl_2$ were incubated with or without 30 mM EDTA at room temperature for 1 h. After washing with TBS, peroxidase-conjugated anti-human IgG antibody (Jackson ImmunoResearch Laboratories, Inc.) was added and incubated at room temperature for 1 h. The binding of Fc-proteins to the NA2 polymers was determined by measuring the absorbance at 450 nm. The NA2 polymer was kindly provided by GlyTech, Inc. (Osaka, Japan).

Serum concentration of calcium ion and TRAP after administration of neuraminidase
WT and *Dcir*$^{-/-}$ male mice 8–12 wk old were intravenously administered with either neuraminidase (0.1 U/mouse; Roche) or PBS five times every second day. 24 h after the last injection, whole blood samples were collected by cardiac puncture under

the anesthesia condition. The serum concentration of calcium ions was determined with the Calcium E-HA test (Wako). The TRAP activity was determined using a TRAPCP & ALP Assay Kit (Takara Bio) by measuring the absorbance at 405 nm.

CIA and neuraminidase treatment

CIA was induced as previously described (Inglis et al., 2008). Briefly, chicken type II collagen (IIC; Sigma-Aldrich) was dissolved in 10 mM of acetic acid (4 mg/ml) overnight at 4°C and stored at –80°C until use. An emulsion was formed by combining CFA (Difco) with an equal volume of the IIC solution (stocked as 4 mg/ml) for DBA/1J mice. IFA (Thermo Fischer Scientific) supplemented with 1 mg/ml of *Mycobacterium tuberculosis* H37Ra (Becton Dickinson Co.) was used for the immunization of C57BL/6J. Mice 8–12 wk old were intradermally immunized with 100 µl of emulsion for DBA/1J or 200 µl for C57BL/6J at three distinct sites in the back, near the base of their tails. A total of 14 d after the first immunization, the mice were intradermally immunized with the same amount of CFA/IIC in the vicinity of the first injection site as a boost. The development of arthritis was monitored for 40 d. The arthritis score was evaluated in each limb according to the following criteria, and the maximal score of arthritis severity was 12 per mouse: 0 = normal, 1 = slight swelling and/or erythema, 2 = severe swelling and/or erythema, and 3 = ankylosis of the joint.

WT and *Dcir*^{−/−} mice were intravenously administered with 100 µl of neuraminidase (2 U/mouse, cloned from *Clostridium perfringens*, NEB [P0720]) or PBS 1 d before the first immunization of CFA/IIA. One day after the first immunization, the mice were intravenously injected with either neuraminidase or PBS, followed by six additional administrations, one every 2 d. DBA/1J mice were intravenously administered with neuraminidase available from Roche (0.1 U/mouse) or PBS.

Measurement of anti-collagen antibody titer

On day 45 after CIA induction, whole blood was obtained by cardiac puncture under anesthesia conditions. The blood samples were left to clot at 4°C for overnight and centrifuged at 3,000 rpm for 10 min to separate serum from coagulated blood. The serum was collected and stored at –80°C until use. IIC (20 µg/ml in PBS) was coated on a 96-well plate at 4°C overnight. The wells were blocked with 10% FBS in PBS at room temperature for 1 h. Serum samples were diluted 5,000-, 2,500-, 500-, 500-, and 100-fold for total IgG, IgG1, IgG2a, IgG2b, and IgG3, respectively. These diluted samples were applied and incubated at room temperature for 2 h. HRP-conjugated goat anti-mouse IgG at 0.8 µg/ml (Jackson ImmunoResearch Laboratories, Inc.) or alkaline phosphatase-conjugated anti-mouse IgG1, IgG2a, IgG2b, and IgG3 at 0.4 µg/ml (Santa Cruz) was added and incubated at room temperature for 1 h. Then, 3, 3′, 5, 5′-tetramethylbenzidine solution (DAKO, Agilent Technologies) for IgG or p-nitrophenyl phosphate solution (Sigma-Aldrich) for IgG1, IgG2a, IgG2b, and IgG3 was added as substrate, and 1 N HCl or 1 N NaOH was used to stop color development. The titers of antibody were determined by measuring the absorbancy of 450 nm for IgG and 405 nm for IgG subclasses.

Measurement of serum cytokine

Sera were prepared as described above, at the end of clinical monitoring of CIA. Using undiluted sera, concentrations of IFN-γ and IL-17 were measured with the mouse ELISA kits (R&D Systems), and the concentration of IL-6 with the mouse ELISA MAX (BioLegend).

Serum concentration of CTX-I

CIA was induced in WT and *Dcir*^{−/−} mice, or DBA/1J mice with or without neuraminidase injection. At the end of observation, whole blood samples were collected by cardiac puncture under an anesthesia condition. The serum concentration of CTX-I was determined with a CTX-I detection ELISA kit using a competitive assay system, according to the manufacturer's procedure (Chondrex, Inc.).

Evaluation of histological arthritic severity and TRAP-positive cells

Two ankle joints of the hind limbs were amputated on day 45 of CIA. The joints were fixed with 10% neutral formalin and decalcified in 10% EDTA. They were embedded in paraffin blocks, and paraffin sections (4 µm) were prepared for H&E staining. Tissue images were taken with NanoZoomer-SQ (Hamamatsu Photonics K.K.). Arthritic severity scores were calculated for the following four parameters: inflammation, pannus formation, cartilage damage, and bone damage. One section from the right and left ankle joint of the hind limbs was evaluated, and each of these parameters has a total of three points for each joint. The criteria of arthritic severity for each parameter are as follows. For inflammation, 0 = normal, 1 = local infiltration of a few inflammatory cells, 2 = broad local infiltration of inflammatory cells, and 3 = broad infiltration into the joint capsule. For pannus formation, 0 = normal, 1 = pannus formation at less than two sites, 2 = pannus formation at less than four sites, and 3 = pannus formation at more than four sites. One broad pannus formation was counted as two sites. For cartilage damage, 0 = normal, 1 = small loss of articular chondrocytes, 2 = cartilage degradation in one region, and 3 = cartilage degradation in more than two regions. For bone damage, 0 = normal, 1 = rough surface of the talus, 2 = shallow loss of the talus, and 3 = deep loss of the talus. Paraffin sections (4 µm) were stained with Naphthol AS-MX phosphate and Fast-Red for 30 min at room temperature. TRAP-positive cells were counted in sections of the right and left ankle joint containing tibia, talus, calcaneus, navicular, cuneiform, metatarsal bones, and phalanges.

EAE and neuraminidase treatment

Mice were subcutaneously immunized with 100 µg of pMOG, which was emulsified in 200 µl of IFA (Thermo Fischer Scientific) and PBS (1:1) supplemented with 500 µg nonviable *M. tuberculosis* H37RA (Difco Laboratories Inc.), on days 0 and 7. The mice were intraperitoneally injected with 200 ng of pertussis toxin (List Biological Labs, Inc.) in PBS on days 0 and 2. Clinical scores of EAE were monitored for 30 d according to the following criteria: 0, no disease; 0.5, partial limp tail; 1, paralyzed tail; 1.5, paralyzed in one hind limb; 2, both hind limbs paralyzed; 2.5, weakness in one forelimb; 3, both forelimbs weakened; 4, forelimbs paralyzed; and 5, moribund. The mean clinical score was determined by averaging the scores of all mice in each group. The cumulative score is the sum of the daily clinical

scores of each individual mouse and indicated as an average of each group. The average maximal score and onset are calculated as an average of the maximal clinical score or date of EAE onset of each individual mouse in each group.

WT and $Dcir^{-/-}$ mice were intravenously administered with 100 µl of neuraminidase (0.1 U/mouse; Roche) or PBS 6 d before the first immunization of pMOG. The mice were intravenously injected with either neuraminidase or PBS, followed by seven further injections administered every 2 d.

Evaluation of histological encephalomyelitic severity

Mice administered with mixed anesthetic agents, containing medetomidine, midazolam, and butorphanol, were intracardially perfused with PBS by drip infusion, followed by perfusion with 10% neutral formalin. Spinal cords were dissected and transferred sequentially into 10% sucrose, 20% sucrose, and then 30% sucrose, at 4°C overnight. The tissues were frozen in Tissue-Tek (Sakura Finteck), and frozen sections (6 µm) between L3 and L5 position were prepared using a microtome (Leica CM3050S; Leica Camera AG). Serial frozen sections were stained with H&E or KB staining, and a double staining with Cresyl violet solution and Luxol fast blue (Muto Pure Chemicals Co. Ltd.), and photos were taken with NanoZoomer-SQ. Four tissue sections were used to evaluate the inflammation severity of the spinal cord. The criteria of encephalomyelitic severity are as follows: 0, no inflammation; 1, cellular infiltration only in the perivascular areas and meninges; 2, mild cellular infiltration in parenchyma (inflammatory cells infiltrated less than one third area of the white matter); 3, moderate cellular infiltration in parenchyma (inflammatory cells infiltrated more than one third area of the white matter); and 4, severe cellular infiltration in parenchyma. Demyelination conditions were assessed by KB staining with the following criteria: 0, no demyelination; 1, mild demyelination; 2, moderate demyelination; and 3, severe demyelination (Okuda et al., 2002; Seno et al., 2015).

Magnetic cell sorting

For the co-culture of 2D2 T cells and DCs, splenic cells were prepared from WT and $Dcir^{-/-}$ mice, and red blood cells were removed by a hemolysis buffer. Resuspended cells were treated with 2.4G2 at 4°C for 15 min to block Fc receptors. After washing with a FACS buffer, the cells were incubated with 15 µl of CD11b- and CD11c-MicroBeads per 10 million cells for 30 min at 4°C. CD11b- and CD11c-positive fractions were separated with an auto MACS Pro separator (Miltenyi Biotec), and these cells were used as antigen-presenting cells.

Cells from the spleens and the auxiliary, branchial, cervical, inguinal, and mesenteric lymph nodes were treated with a hemolysis buffer to remove red blood cells. The Fc receptors on these cells were blocked with 2.4G2 at 4°C for 15 min, and the cells were incubated with 10 µl of Thy1.2 MicroBeads per 10 million total cells for 30 min at 4°C. Thy1.2-positive fractions were separated with an auto MACS Pro separator, and these cells were used as 2D2 T cells.

2D2 T cell–DC co-culture and T cell proliferation assay

2D2 T cells (2×10^5 cells) were cultured either with WT or $Dcir^{-/-}$ DCs (2×10^4 cells) with or without pMOG (10 µg/ml and 100 µg/ml) for 3 d in a 96-well round-bottom plate in RPMI supplemented with 0.1 mM of β-mercaptoethanol, 100 U/ml of penicillin, 100 µg/ml of streptomycin, and 10% heat-inactivated FBS (the culture medium is called as R10). 2D2 T cells and DCs were sorted with the auto MACS Pro separator described above. Neuraminidase (Roche) was added at the concentration of 0.1 mU/ml at the start of the culture (day 0) and the day after the culture was started (day 1). For the assay of NA2-mediated inhibition, a 96-well plate was coated with 2 µg/ml NA2-BSA or BSA at 4°C for overnight. The plate was washed twice with PBS before it was used. The cells were subjected to the cell surface and intracellular staining for FACS analysis.

For T cell proliferation assay, 2D2 T cells (2×10^5 cells) and DCs (4×10^4 cells) were co-cultured for 3 d with pMOG (10 µg/ml) with or without neuraminidase (0.01 mU/ml; Roche). The cell proliferation was determined with a colorimetric immunoassay based on the incorporation of BrdU, according to the manufacturer's procedure (Roche). Briefly, 3 d after initiating with the co-culture, BrdU (final concentration was 10 µM) was added, and the cells were incubated for additional 6 h. The cells were fixed, and the DNA was denatured at room temperature. After removing the fixing and denaturation solution, the anti-BrdU-POD antibody was added and reacted for 90 min at room temperature. The BrdU incorporation was determined by measuring the absorbance of 450 nm with a reference wavelength of 570 nm.

GM-DC culture

BMCs were isolated by flushing the BM cavity of the femurs and tibias with R10. Red blood cells were destroyed in a hemolysis buffer for 10 min on ice. The BMCs were cultured at the concentration of 2×10^6 cells in 10 ml R10 in a nontreated 100-mm dish with 20 ng/ml of GM-CSF (Peprotech). 3 d after incubation, 10 ml of R10 containing 20 ng/ml of GM-CSF was added to the dish. At 6 and 8 d, 10 ml of supernatant was collected, and the cell pellet, after centrifugation at 1,500 rpm for 5 min, was resuspended with an equal volume of R10 containing 20 ng/ml of GM-CSF, followed by the restoration of the suspension into the dish. At 10 d, cells in the supernatant were used as GM-DCs.

2D2 T cell activation with anti-CD3 and anti-CD28 antibodies

Thy1.2$^+$ cells from spleens and lymph nodes were sorted with an auto MACS Pro separator (Miltenyi Biotec). Anti-CD3 antibody (10 µg/ml; Biolegend) was coated on a 96-well plate at 4°C for overnight. The Thy1.2$^+$ cells were seeded at 2×10^5 cells per well with soluble anti-CD28 antibody (2 µg/ml) and cultured at 37°C for 3 d. The supernatants were stored before used for the detection of cytokines by ELISA. For the staining of intracellular molecules, cells were treated with 2.4G2 (Fc blocker) on ice for 30 min. These cells were permeabilized with fixation/permeabilization solution (BD Biosciences) on ice for 30 min and stained with antibodies against GM-CSF, IFN-γ, IL-17, and Ki67, and analyzed by FACS.

RNA-seq analysis

CD11c$^+$ cells were isolated from the co-culture system with 2D2 T cells in the presence of pMOG (100 µg/ml) for 3 d using an

autoMACS proseparator and were exposed to CellCover (ANACYTE Laboratories) to protect RNA. The purity of the cell population was 95% or more in the FACS analysis. RNA samples were extracted using NucleoSpin RNA XS (Takara Bio), and the RNA quality was assessed by RNA Screen Tape in TapeStation System (Agilent Technologies) to ensure an RNA integrity number >7.0. RNA-seq library construction followed by next-generation sequencing were conducted by GENE-WIZ. Briefly, the total RNA was quantified by a Qubit RNA Assay (Invitrogen) and qualified in the TapeStation system. 25 ng of total RNA was used for mRNA enrichment of poly(A) selection with NEBNext Poly(A) mRNA Magnetic Isolation Module (New England BioLabs). mRNA samples were fragmented and reverse-transcribed for the first strand and second strand cDNA using random primers. The 5′ and/or 3′ ends of the fragmented RNA were repaired, and indexed adaptors were added via ligation. RNA-seq libraries were prepared using a MGIEasy RNA Directional Library Prep Set V2.0 (MGI Tech) according to the manufacturer's instructions. The generated libraries were quantified by Qubit DNA Assay, and the fragment size was assayed by D1000 DNA Screen Tape in TapeStation. Libraries with unique sample barcodes were pooled and sequenced using DNBSEQ-G400 (MGI Tech) in a 150-bp paired-end configuration. Approximately 20 million paired-end reads per sample were yielded, and nearly 90% of the sequence had a Q30 score.

RNA-seq data processing
The raw sequencing data were processed using TrimGalore v0.6.6 to remove adapter sequences and low-quality reads. The processed reads were used to align to the mouse genome reference mm10 using hisat2 v2.2.0. Aligned read counts that fell on the exons of each gene were calculated by the R package Rsubread v1.32.4. The read counts were normalized and compared for differential gene expression using R package edgeR v3.24.3. The RNA-seq data have been deposited in the Gene Expression Omnibus database under accession no. GSE184068.

Functional signatures of changes in gene expression in DCs
A GO enrichment analysis was performed by the PANTHER Overrepresentation Test (Released 20200728) for the analysis of functional pathways. Differentially expressed genes that were fold-change >0 and P value <0.05 were selected for the GO enrichment analysis. The functional signatures of gene sets were recategorized as below. Genes annotated with the MHCII protein complex, antigen processing and presentation, and the regulation of T cell proliferation were described as antigen presentation and T cell proliferation. Genes annotated with a pattern recognition receptor signaling pathway and a transmembrane receptor protein tyrosine kinase signaling pathway were described as receptor signaling pathways.

Statistics
The statistical significance between groups was determined using the two-tailed unpaired Student's t test (*, $P < 0.05$; **, $P < 0.01$; ***, $P < 0.001$). The clinical and histological scores of CIA and EAE were evaluated using the Mann–Whitney U test or one-way ANOVA with Dunnett's post hoc test, and the incidence of CIA and EAE was analyzed using the χ^2 test. The difference between the groups was considered statistically significant at $P < 0.05$.

Online supplemental material
Fig. S1 shows the binding of DCIR to N-linked glycans on macrophages, osteoclasts, and osteoblasts in a CRD- and Ca^{2+}-dependent manner. Fig. S2 provides the data of DCIR-Fc or Fc-protein binding on a glycan array and shows DCIR expression in macrophages and OsteoMacs. Fig. S3 shows the effect of intravenous administration of neuraminidase on DCIR-Fc binding to BMCs. In addition, the production of anti-collagen antibody is comparable in CIA-induced mice with neuraminidase treatment. Fig. S4 provides flow cytometry data of cytokine production from T cells stimulated with pMOG in neuraminidase treatment. Fig. S5 shows cytokine production from T cells activated with anti-CD3/CD28 antibody after neuraminidase treatment. Table S1 lists the antibodies. Table S2 shows PCR primer sets.

References
Bloem, K., I.M. Vuist, A.J. van der Plas, L.M. Knippels, J. Garssen, J.J. García-Vallejo, S.J. van Vliet, and Y. van Kooyk. 2013. Ligand binding and signaling of dendritic cell immunoreceptor (DCIR) is modulated by the glycosylation of the carbohydrate recognition domain. *PLoS One.* 8: e66266. https://doi.org/10.1371/journal.pone.0066266

Bloem, K., I.M. Vuist, M. van den Berk, E.J. Klaver, I. van Die, L.M. Knippels, J. Garssen, J.J. García-Vallejo, S.J. van Vliet, and Y. van Kooyk. 2014. DCIR interacts with ligands from both endogenous and pathogenic origin. *Immunol. Lett.* 158:33–41. https://doi.org/10.1016/j.imlet.2013.11.007

Bookout, A.L., and D.J. Mangelsdorf. 2003. Quantitative real-time PCR protocol for analysis of nuclear receptor signaling pathways. *Nucl. Recept. Signal.* 1:e012. https://doi.org/10.1621/nrs.01012

Brand, D.D., K.A. Latham, and E.F. Rosloniec. 2007. Collagen-induced arthritis. *Nat. Protoc.* 2:1269–1275. https://doi.org/10.1038/nprot.2007.173

Chang, M.K., L.J. Raggatt, K.A. Alexander, J.S. Kuliwaba, N.L. Fazzalari, K. Schroder, E.R. Maylin, V.M. Ripoll, D.A. Hume, and A.R. Pettit. 2008. Osteal tissue macrophages are intercalated throughout human and mouse bone lining tissues and regulate osteoblast function in vitro and in vivo. *J. Immunol.* 181:1232–1244. https://doi.org/10.4049/jimmunol.181.2.1232

Crocker, P.R., J.C. Paulson, and A. Varki. 2007. Siglecs and their roles in the immune system. *Nat. Rev. Immunol.* 7:255–266. https://doi.org/10.1038/nri2056

Fujikado, N., S. Saijo, T. Yonezawa, K. Shimamori, A. Ishii, S. Sugai, H. Kotaki, K. Sudo, M. Nose, and Y. Iwakura. 2008. Dcir deficiency causes development of autoimmune diseases in mice due to excess expansion of dendritic cells. *Nat. Med.* 14:176–180. https://doi.org/10.1038/nm1697

Graham, L.M., and G.D. Brown. 2009. The Dectin-2 family of C-type lectins in immunity and homeostasis. *Cytokine.* 48:148–155. https://doi.org/10.1016/j.cyto.2009.07.010

Hoffmann, A., S. Kerr, J. Jellusova, J. Zhang, F. Weisel, U. Wellmann, T.H. Winkler, B. Kneitz, P.R. Crocker, and L. Nitschke. 2007. Siglec-G is a B1 cell-inhibitory receptor that controls expansion and calcium signaling of the B1 cell population. *Nat. Immunol.* 8:695–704. https://doi.org/10.1038/ni1480

Hsu, T.L., S.C. Cheng, W.B. Yang, S.W. Chin, B.H. Chen, M.T. Huang, S.L. Hsieh, and C.H. Wong. 2009. Profiling carbohydrate-receptor interaction with recombinant innate immunity receptor-Fc fusion proteins. *J. Biol. Chem.* 284:34479–34489. https://doi.org/10.1074/jbc.M109.065961

Inglis, J.J., E. Simelyte, F.E. McCann, G. Criado, and R.O. Williams. 2008. Protocol for the induction of arthritis in C57BL/6 mice. *Nat. Protoc.* 3:612–618. https://doi.org/10.1038/nprot.2008.19

Kaifu, T., J. Nakahara, M. Inui, K. Mishima, T. Momiyama, M. Kaji, A. Sugahara, H. Koito, A. Ujike-Asai, A. Nakamura, et al. 2003. Osteopetrosis and thalamic hypomyelinosis with synaptic degeneration in DAP12-deficient mice. *J. Clin. Invest.* 111:323–332. https://doi.org/10.1172/JCI16923

Kameda, Y., M. Takahata, M. Komatsu, S. Mikuni, S. Hatakeyama, T. Shimizu, T. Angata, M. Kinjo, A. Minami, and N. Iwasaki. 2013. Siglec-15 regulates osteoclast differentiation by modulating RANKL-induced phosphatidylinositol 3-kinase/Akt and Erk pathways in association with signaling Adaptor DAP12. *J. Bone Miner. Res.* 28:2463–2475. https://doi.org/10.1002/jbmr.1989

Koga, T., M. Inui, K. Inoue, S. Kim, A. Suematsu, E. Kobayashi, T. Iwata, H. Ohnishi, T. Matozaki, T. Kodama, et al. 2004. Costimulatory signals mediated by the ITAM motif cooperate with RANKL for bone homeostasis. *Nature.* 428:758–763. https://doi.org/10.1038/nature02444

Lee, Y.M., N. Fujikado, H. Manaka, H. Yasuda, and Y. Iwakura. 2010. IL-1 plays an important role in the bone metabolism under physiological conditions. *Int. Immunol.* 22:805–816. https://doi.org/10.1093/intimm/dxq431

Lee, R.T., T.L. Hsu, S.K. Huang, S.L. Hsieh, C.H. Wong, and Y.C. Lee. 2011. Survey of immune-related, mannose/fucose-binding C-type lectin receptors reveals widely divergent sugar-binding specificities. *Glycobiology.* 21:512–520. https://doi.org/10.1093/glycob/cwq193

Livak, K.J., and T.D. Schmittgen. 2001. Analysis of relative gene expression data using real-time quantitative PCR and the 2(-Delta Delta C(T)) Method. *Methods.* 25:402–408. https://doi.org/10.1006/meth.2001.1262

Ma, D.Y., and E.A. Clark. 2009. The role of CD40 and CD154/CD40L in dendritic cells. *Semin. Immunol.* 21:265–272. https://doi.org/10.1016/j.smim.2009.05.010

Maruhashi, T., T. Kaifu, R. Yabe, A. Seno, S.H. Chung, N. Fujikado, and Y. Iwakura. 2015. DCIR maintains bone homeostasis by regulating IFN-γ production in T cells. *J. Immunol.* 194:5681–5691. https://doi.org/10.4049/jimmunol.1500273

Massoud, A.H., M. Yona, D. Xue, F. Chouiali, H. Alturaihi, A. Ablona, W. Mourad, C.A. Piccirillo, and B.D. Mazer. 2014. Dendritic cell immunoreceptor: a novel receptor for intravenous immunoglobulin mediates induction of regulatory T cells. *J. Allergy Clin. Immunol.* 133:853–863.e5. https://doi.org/10.1016/j.jaci.2013.09.029

Nagae, M., A. Ikeda, S. Hanashima, T. Kojima, N. Matsumoto, K. Yamamoto, and Y. Yamaguchi. 2016. Crystal structure of human dendritic cell inhibitory receptor C-type lectin domain reveals the binding mode with N-glycan. *FEBS Lett.* 590:1280–1288. https://doi.org/10.1002/1873-3468.12162

Nasu, J., T. Uto, T. Fukaya, H. Takagi, T. Fukui, N. Miyanaga, Y. Nishikawa, S. Yamasaki, Y. Yamashita, and K. Sato. 2020. Pivotal role of the carbohydrate recognition domain in self-interaction of CLEC4A to elicit the ITIM-mediated inhibitory function in murine conventional dendritic cells in vitro. *Int. Immunol.* 32:673–682. https://doi.org/10.1093/intimm/dxaa034

Negishi-Koga, T., M. Shinohara, N. Komatsu, H. Bito, T. Kodama, R.H. Friedel, and H. Takayanagi. 2011. Suppression of bone formation by osteoclastic expression of semaphorin 4D. *Nat. Med.* 17:1473–1480. https://doi.org/10.1038/nm.2489

Nitschke, L. 2005. The role of CD22 and other inhibitory co-receptors in B-cell activation. *Curr. Opin. Immunol.* 17:290–297. https://doi.org/10.1016/j.coi.2005.03.005

Okamoto, K., and H. Takayanagi. 2019. Osteoimmunology. *Cold Spring Harb. Perspect. Med.* 9:a031245. https://doi.org/10.1101/cshperspect.a031245

Okuda, Y., M. Okuda, and C.C. Bernard. 2002. The suppression of T cell apoptosis influences the severity of disease during the chronic phase but not the recovery from the acute phase of experimental autoimmune encephalomyelitis in mice. *J. Neuroimmunol.* 131:115–125. https://doi.org/10.1016/S0165-5728(02)00267-9

Pederson, L., M. Ruan, J.J. Westendorf, S. Khosla, and M.J. Oursler. 2008. Regulation of bone formation by osteoclasts involves Wnt/BMP signaling and the chemokine sphingosine-1-phosphate. *Proc. Natl. Acad. Sci. USA.* 105:20764–20769. https://doi.org/10.1073/pnas.0805133106

Regoeczi, E., P. Taylor, M.T. Debanne, L. März, and M.W. Hatton. 1979. Three types of human asialo-transferrin and their interactions with the rat liver. *Biochem. J.* 184:399–407. https://doi.org/10.1042/bj1840399

Richard, M., N. Thibault, P. Veilleux, G. Gareau-Pagé, and A.D. Beaulieu. 2006. Granulocyte macrophage-colony stimulating factor reduces the affinity of SHP-2 for the ITIM of CLECSF6 in neutrophils: a new mechanism of action for SHP-2. *Mol. Immunol.* 43:1716–1721. https://doi.org/10.1016/j.molimm.2005.10.006

Seno, A., T. Maruhashi, T. Kaifu, R. Yabe, N. Fujikado, G. Ma, T. Ikarashi, S. Kakuta, and Y. Iwakura. 2015. Exacerbation of experimental autoimmune encephalomyelitis in mice deficient for DCIR, an inhibitory C-type lectin receptor. *Exp. Anim.* 64:109–119. https://doi.org/10.1538/expanim.14-0079

Stanley, P., V. Caillibot, and L. Siminovitch. 1975. Selection and characterization of eight phenotypically distinct lines of lectin-resistant Chinese hamster ovary cell. *Cell.* 6:121–128. https://doi.org/10.1016/0092-8674(75)90002-1

Stromnes, I.M., and J.M. Goverman. 2006. Active induction of experimental allergic encephalomyelitis. *Nat. Protoc.* 1:1810–1819. https://doi.org/10.1038/nprot.2006.285

Takahata, M., N. Iwasaki, H. Nakagawa, Y. Abe, T. Watanabe, M. Ito, T. Majima, and A. Minami. 2007. Sialylation of cell surface glycoconjugates is essential for osteoclastogenesis. *Bone.* 41:77–86. https://doi.org/10.1016/j.bone.2007.03.016

Takeshita, S., N. Namba, J.J. Zhao, Y. Jiang, H.K. Genant, M.J. Silva, M.D. Brodt, C.D. Helgason, J. Kalesnikoff, M.J. Rauh, et al. 2002. SHIP-deficient mice are severely osteoporotic due to increased numbers of hyper-resorptive osteoclasts. *Nat. Med.* 8:943–949. https://doi.org/10.1038/nm752

Tateno, H., A. Mori, N. Uchiyama, R. Yabe, J. Iwaki, T. Shikanai, T. Angata, H. Narimatsu, and J. Hirabayashi. 2008. Glycoconjugate microarray based on an evanescent-field fluorescence-assisted detection principle for investigation of glycan-binding proteins. *Glycobiology.* 18:789–798. https://doi.org/10.1093/glycob/cwn068

Thiemann, S., and L.G. Baum. 2016. Galectins and Immune Responses-Just How Do They Do Those Things They Do? *Annu. Rev. Immunol.* 34:243–264. https://doi.org/10.1146/annurev-immunol-041015-055402

Umeda, S., W.G. Beamer, K. Takagi, M. Naito, S. Hayashi, H. Yonemitsu, T. Yi, and L.D. Shultz. 1999. Deficiency of SHP-1 protein-tyrosine phosphatase activity results in heightened osteoclast function and decreased bone density. *Am. J. Pathol.* 155:223–233. https://doi.org/10.1016/S0002-9440(10)65116-4

Yang, W.H., C. Nussbaum, P.K. Grewal, J.D. Marth, and M. Sperandio. 2012. Coordinated roles of ST3Gal-VI and ST3Gal-IV sialyltransferases in the synthesis of selectin ligands. *Blood.* 120:1015–1026. https://doi.org/10.1182/blood-2012-04-424366

Zelensky, A.N., and J.E. Gready. 2005. The C-type lectin-like domain superfamily. *FEBS J.* 272:6179–6217. https://doi.org/10.1111/j.1742-4658.2005.05031.x

Zhang, M., T. Angata, J.Y. Cho, M. Miller, D.H. Broide, and A. Varki. 2007. Defining the in vivo function of Siglec-F, a CD33-related Siglec expressed on mouse eosinophils. *Blood.* 109:4280–4287. https://doi.org/10.1182/blood-2006-08-039255
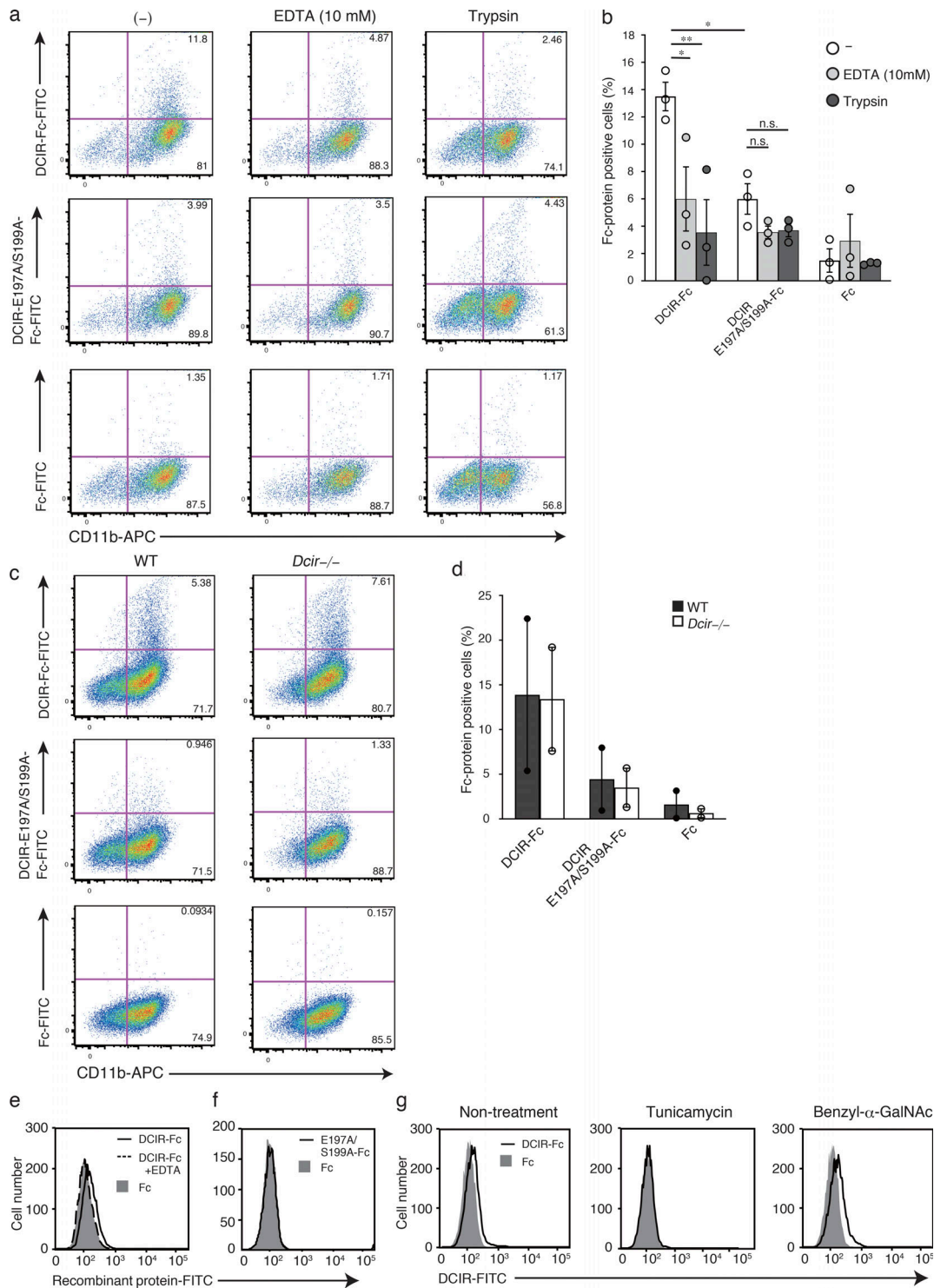
Supplemental material

Figure S1. **DCIR binds to N-linked glycans on macrophages, osteoclasts, and osteoblasts in a CRD- and Ca²⁺-dependent manner. (a and b)** DCIR-Fc binding to in vitro differentiated CD11b⁺ mature macrophages (6 d culture with M-CSF) with or without EDTA and trypsin treatment was analyzed by flow cytometry. DCIR-Fc was preincubated with FITC–anti-human IgG, and the cells were stained with the FITC–anti-human-IgG-labeled DCIR-Fc (DCIR-Fc-FITC) and APC-labeled anti-CD11b antibody (CD11b-APC). Representative flow cytometry plots of CD11b⁺ mature macrophages. Data denote the mean ± SEM of three independent experiments. Statistical significances (*, P < 0.05; **, P < 0.01) are evaluated by the two-tailed paired Student's t test. **(c and d)** CD11b⁺ osteoclasts were induced to differentiate from WT and Dcir⁻/⁻ BMMs by treating with M-CSF and RANKL. Then the binding of DCIR-Fc, mutant DCIR-Fc, and Fc protein was examined with a flow cytometer at 5 d after induction of differentiation. Comparable DCIR-Fc binding was observed between WT and Dcir⁻/⁻ osteoclasts. Representative flow cytometry plots of CD11b⁺ osteoclasts. The data are representative of two independent experiments. Data denote the average ± SD of two independent experiments. **(e)** DCIR-Fc binding to osteoblasts with or without EDTA. **(f)** DCIR-Fc or mutant DCIR-Fc binding to osteoblasts. **(g)** The effects of tunicamycin and benzyl-α-GalNAc, which inhibits N-linked glycosylation and O-linked glycosylation, respectively, on DCIR-Fc binding to osteoblasts were examined. The data are representative of two independent experiments (e–g).
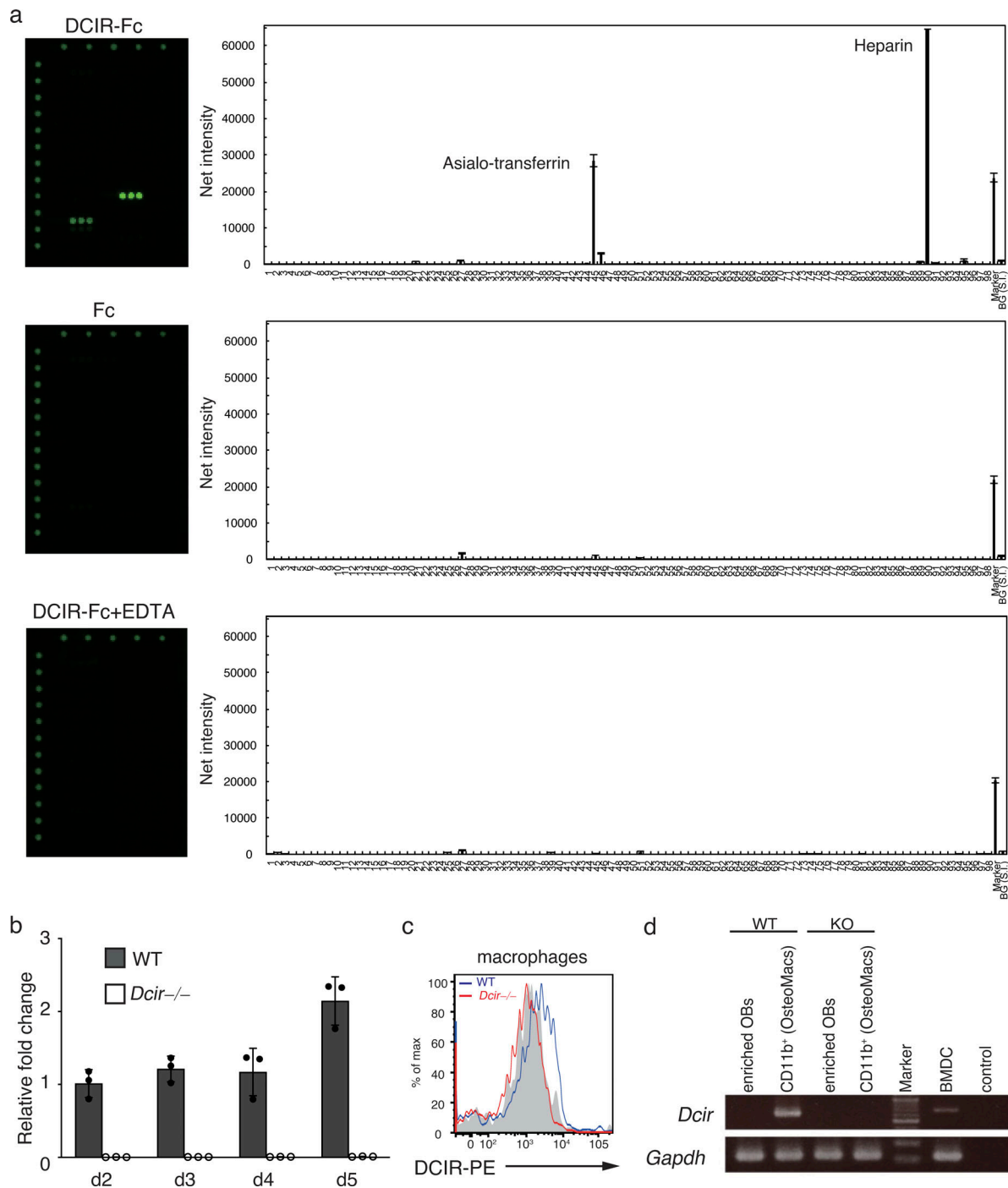
Figure S2. Analysis of DCIR ligands on a glycan array and DCIR expression in macrophages and OsteoMacs. (a) Binding of DCIR-Fc (10 µg/ml) or Fc-protein to a glycan array was assessed in the presence or absence of EDTA as described in the Materials and methods. Binding was detected with an evanescence-field fluorescence-activated scanner. Positive spots are asialo-transferrin and heparin. The experiment was performed twice. **(b)** BMMs were induced to differentiate from BMCs using M-CSF, and *Dcir* mRNA was quantified by real-time PCR at the indicated days. Relative expressions at day 2 are shown. **(c)** DCIR expression on BMM cell surface was analyzed at day 4 with a flow cytometer. WT and *Dcir*⁻/⁻ macrophages are indicated by blue and red lines, respectively, and isotype control is indicated in gray. **(d)** Calvaria cells gained from neonates were purified as CD11b⁺ cells (OsteoMacs) and CD11b- cells (osteoblasts [OBs]) with an autoMACS, and *Dcir* expression was analyzed by conventional PCR. BMDCs were used as a positive control. The results are representative of at least three independent experiments (b–d).
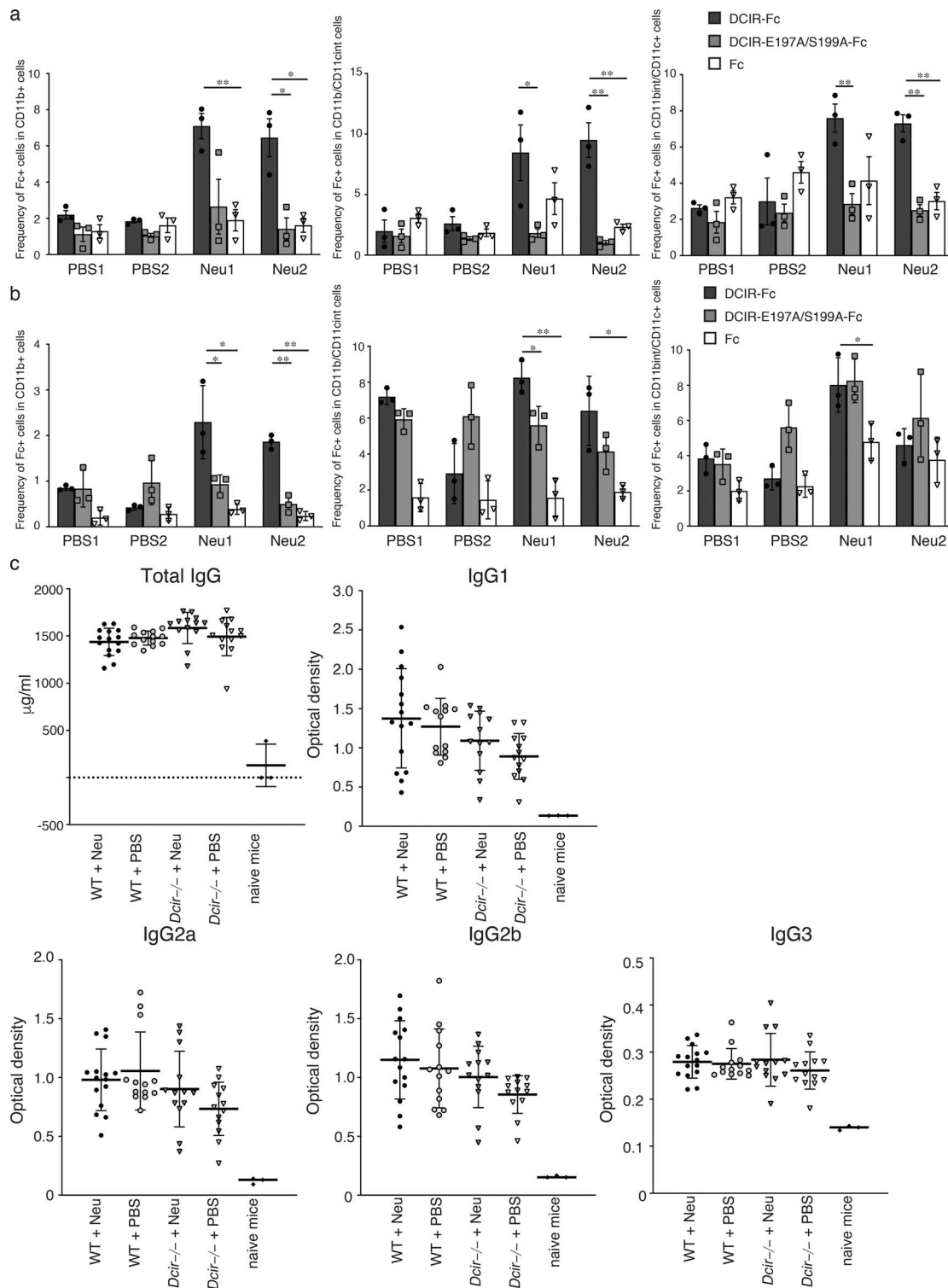
Figure S3. **Intravenous administration of neuraminidase increases DCIR-Fc binding to BMCs, but neuraminidase treatment does not affect anti-collagen antibody levels in CIA-induced mice. (a)** Neuraminidase (Neu; 0.2 U/mouse, *n* = 2) or PBS (*n* = 2) was intravenously injected into WT mice, and BMCs were prepared 24 h after the administration. Binding of DCIR-Fc to three distinct populations of BMCs (CD11b+, CD11b+/CD11cint, CD11bint/CD11c+) was analyzed by FACS. **(b)** DCIR-Fc binding to BMCs was analyzed at 48 h after neuraminidase administration. DCIR-Fc binding was evaluated in three independent FACS trials from one mouse, and the bars represent the mean ± SD of triplicate bindings. One experiment used two mice each for PBS and neuraminidase, and two independent experiments are shown (a and b). Statistical significances (*, P < 0.05; **, P < 0.01) are evaluated by the one-way ANOVA with Dunnett's post hoc test. **(c)** Anti-collagen antibody titers after neuraminidase treatment. Sera were collected from neuraminidase- and PBS-treated mice at day 42 after immunization. Anti-type II collagen antibody titers were measured by ELISA, using sera collected from mice at day 42 after immunization. Neuraminidase-treated mice; solid circle: WT (*n* = 15), inverted triangle: *Dcir*−/− (*n* = 13). PBS-treated mice; circle: WT (*n* = 13), inverted triangle: *Dcir*−/− (*n* = 13). No statistical significance was detected (one-way ANOVA with Dunnett's post hoc test). These assays were performed with sera from one experiment.
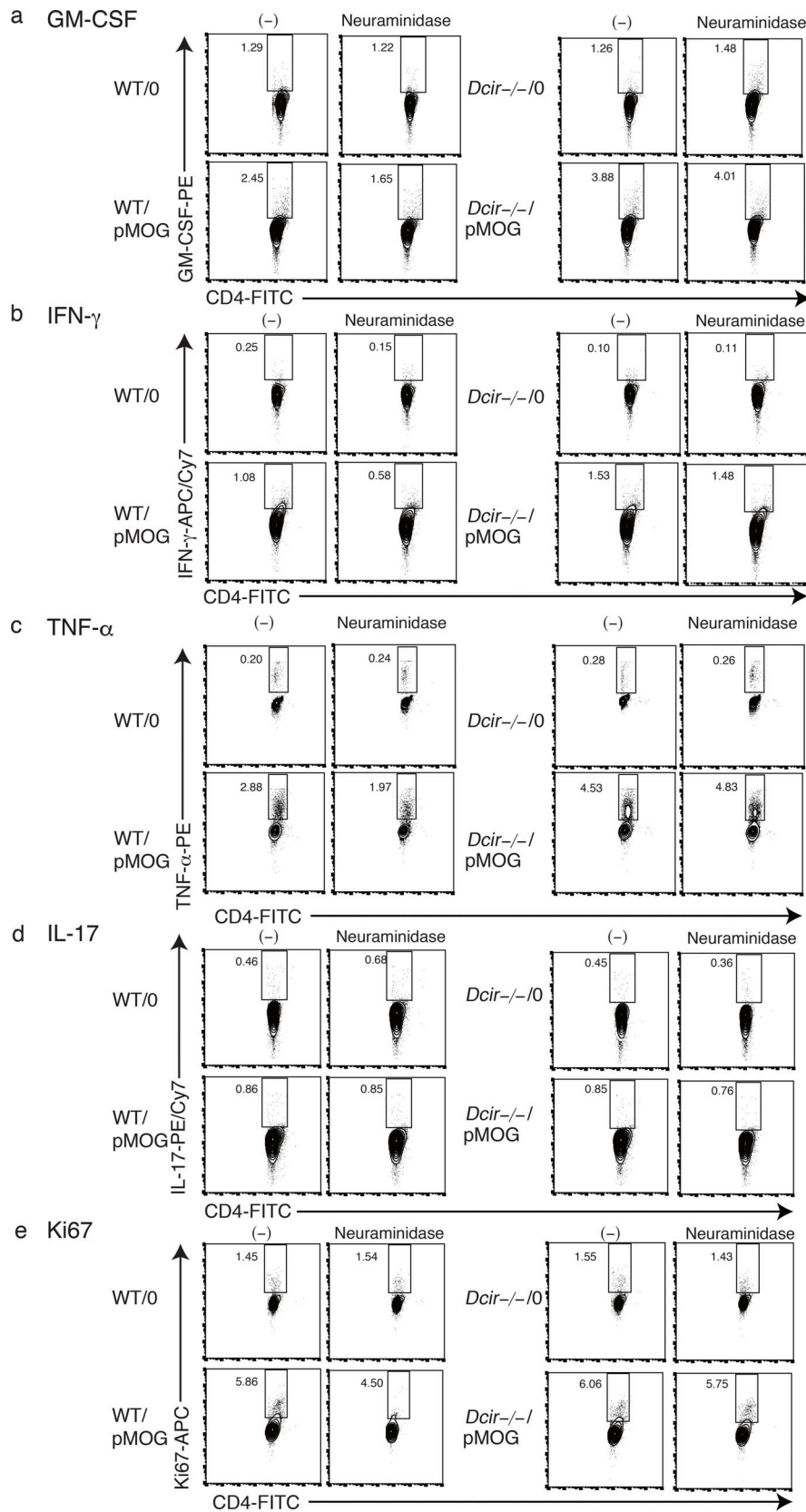
Figure S4. Neuraminidase treatment decreased cytokine production from T cells. Cytokine-positive CD4+ 2D2 T cells co-cultured either with WT or Dcir−/− DCs in the presence or absence of neuraminidase (0.1 mU/ml; Roche) added at days 1 and 2 were examined by FACS after 3 d. The cells were also cultured with or without pMOG. **(a–e)** Representative flow cytometry plots are shown: GM-CSF+CD4+ 2D2T cells (a), IFN-γ+ CD4+ 2D2T cells (b), TNF-α+ CD4+ 2D2T cells (c), IL17+CD4+ 2D2T cells (d), and Ki67+ CD4+ 2D2T cells (e). The data are representative of two independent experiments (a–e).
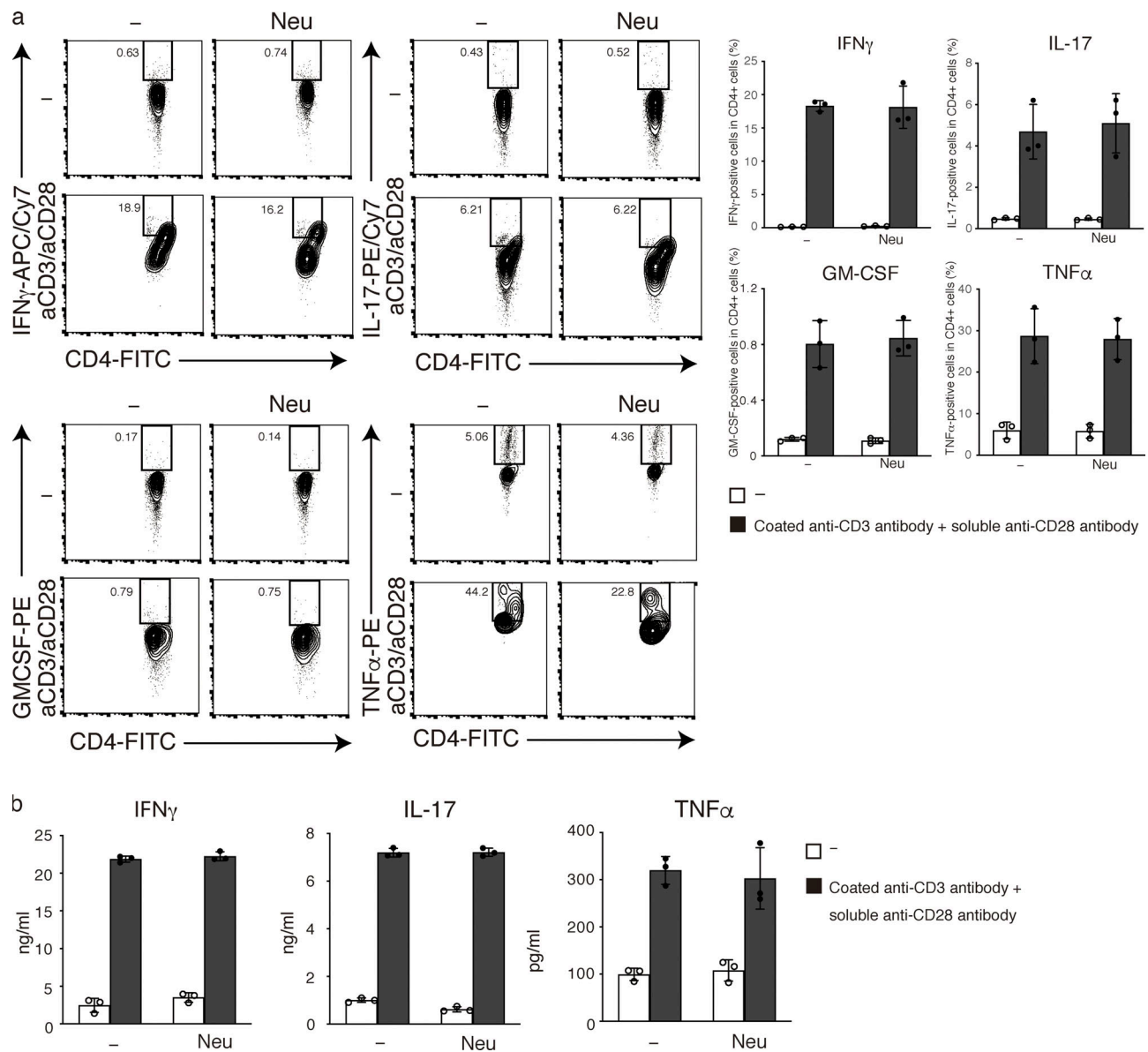
Figure S5. **Neuraminidase treatment does not affect cytokine production in activated T cells. (a)** Thy1.2$^+$ T cells were sorted from the spleen and lymph nodes of 2D2 mice, and stimulated with coated anti-CD3 and soluble anti-CD28 antibodies in the presence or absence of neuraminidase (Neu; 0.1 mU/ml; Roche), added at days 0 and 1. Then the content of cytokine positive cells was measured by FACS at day 3. **(b)** Quantification of cytokines from 2D2 T cells after stimulation with plate-coated anti-CD3 and soluble anti-CD28 antibodies. Data are the mean ± SD of triplicate cultures (a and b). Open bars: isotype control, closed bars: coated anti-CD3 and soluble anti-CD28 antibody.

Table S1 and Table S2 are provided online as separate files. Table S1 lists the antibodies. Table S2 shows PCR primer sets.